EFFECTS OF SOIL TRANSPORT PROCESSES ON ORGANIC CARBON STORAGE IN FORESTED HILLSLOPE SOILS

By

John Coley Roseberry

Thesis

Submitted to the Faculty of the

Graduate School of Vanderbilt University

in the partial fulfillment of the requirements

for the degree of

MASTER OF SCIENCE

in

Earth and Environmental Sciences

May, 2009

Nashville, Tennessee

Approved:

Professor David J. Furbish

Professor Guilherme Gualda

To my wife, Hannah

And my mother, Delores

ACKNOWLEDGMENTS

First and foremost, I would like to thank my advisor, David Furbish, whose guidance and support made this thesis possible. David's curiosity and enthusiasm for the Earth sciences are extraordinary and they kept me pressing forward when things got tough. If everyone were as happy as David is when he looks at a model simulation of hillslope evolution, the world would be a much better place. Thank-you, David.

I extend my appreciation to Virginia Batts, Chelsea Furbish, and Logan Bender for assistance with field work. Thank-you to Susan Howell for help with analytical and field equipment. I appreciate the assistance I received from my thesis committee, Guil Gualda and Steve Goodbred, all of the Earth and Environmental Sciences faculty, and Aaron Covey.

I am thankful for the love and support from family and friends throughout my time working on this thesis. To my lovely wife, who was forced to hear about soil processes, who removed countless ticks from me after field work, and who was supportive during this entire process, thank-you for being there when I needed you.

This work was funded by a Geological Society of America student research grant and the Vanderbilt University Department of Earth and Environmental Sciences.

TABLE OF CONTENTS

Page

DEDICATION ii

ACKNOWLEDGMENTS iii

LIST OF FIGURES vi

Chapter

I. INTRODUCTION 1

II. THEORETICAL MASS-BALANCE MODEL 6

III. METHODS 12

- Field Site 12
- Topographic Surveying 15
- Soil Pits and Sampling 17
- Sample Processing and Analysis 18

IV. RESULTS 20

- Field Results 20
- Modeling Results 37
  - Model Parameterization 37
  - Initial Condition 41
  - Flux of Organic Carbon Across Soil Surface 41
  - Overall Trends in Hillslope Relaxation Simulations 42
  - Soil Production 44
  - *e*-folding Depths of Organic Carbon Production and Respiration 47
  - Diffusion Coefficient 47
  - Incision 52
  - Comparison of Modeled and Measured Soil Organic Carbon 52
  - The Role of Physical Processes on Soil Carbon Cycling 54

V. CONCLUSIONS 58

Appendix

A. SUMMARY OF SOIL PIT DATA 60

B. MATLAB CODE 66

C. DETAILED DIRECTIONS TO FIELD AREA 71

REFERENCES 72

LIST OF FIGURES

Figure Page

1. The carbon cycle on forested hillslopes 2

2. Conceptual model 3

3. Location map and digital elevation model of the field area 13

4. Calculation of hillslope curvature for irregularly spaced data 16

5. Infiltration rates measured at the Middle hillslope using a single-ring infiltrometer 21

6. Photographs of tree throw and LBL 22

7. Photographs of a worm and worm tube from soil pit 08JR05 on the Middle hillslope 22

8. Location of survey transects and transects plotted to scale 23

9. Hillslope curvature of the Upper, Middle, and Lower hillslopes 24

10. Plots of the mass fraction of clasts >2mm 26

11. Plots of soil bulk density versus depth 28

12. Location of soil pits plotted on transect survey, photographs of soil samples, and plot of percent organic carbon versus depth for the Upper hillslope 30

13. Location of soil pits plotted on transect survey, photographs of soil samples, and plot of percent organic carbon versus depth for the Middle hillslope 31

14. Location of soil pits plotted on transect survey, photographs of soil samples, and plot of percent organic carbon versus depth for the Lower hillslope 32

15. Plots of percent soil organic carbon versus depth 33

16. Plots of C:N ratio versus depth, percent nitrogen versus depth, and percent organic carbon versus C:N ratio 34

17. Plots of soil organic carbon storage at sampled intervals versus distance from hillslope crest 35

18. Plot of soil organic carbon storage versus hillslope curvature and distance from hillslope crest 36

19. Precipitation intensity-duration-frequency curves for Dover, Tennessee 38

20. The effect of initial land surface roughness on organic carbon storage over short timescales 43

21. The effect of organic carbon flux across soil surface on SOC storage after 10 ka 43

22. Plots of elevation, SOC storage, and soil thickness versus distance from hillslope crest showing the effect of SOC storage in thinned and thickened soils over 100 ka 45

23. Plots of elevation, SOC storage, and soil thickness versus distance from hillslope crest showing the effect of initial soil production on SOC storage over 100 ka 46

24. Plots of elevation, SOC storage, and soil thickness versus distance from hillslope crest showing the effect of α and β on SOC storage over 100 ka 48

25. Plots of elevation, SOC storage, and soil thickness versus distance from hillslope crest showing the effect of increased diffusion coefficient on SOC storage over 100 ka 49

26. Plots of elevation, SOC storage, and soil thickness versus distance from hillslope crest showing the effect of linearly increasing the diffusion coefficient with distance from hillslope crest on SOC storage over 100 ka 51

27. Plots of elevation, SOC storage, and soil thickness versus distance from hillslope crest showing the effect of incision on SOC storage over 1 Ma 53

28. Plot of curvature versus SOC storage for model simulations presented in Figure 22 and Figure 26 55

CHAPTER I

INTRODUCTION

Concern over the effect of increasing concentrations of atmospheric carbon dioxide on climate change (e.g. IPCC, 2007) has encouraged research on identifying and quantifying carbon dioxide sources and sinks in the global carbon cycle. Presently, models cannot account for the sequestration of 1-2 Gt C yr^{-1} from anthropogenically mobilized CO_2, the so-called "missing sink" (Sundquist, 1993). The recognition and protection of unidentified or underestimated carbon sinks is important in utilizing these sinks in the management of atmospheric CO_2 levels. This thesis investigates the influence of physical soil transport processes on the cycling of organic carbon on forested hillslopes.

Consider the carbon cycle on the scale of a forested hillslope (Figure 1). Atmospheric CO_2 is taken up by plants in photosynthesis, storing carbon in biomass (leaves, stems, and roots). As plants die or seasonally shed leaves, biomass is delivered to the soil surface, in the case of leaves and twigs, or incorporated within the soil profile at depth, as is the case for roots. The biomass entering a soil is subject to the same physical transport processes that are acting on the soil in addition to the biological processes responsible for decomposition (Figure 2).

Stallard (1998) first suggested that human-induced erosion and subsequent deposition of soil may lead to a previously unrecognized carbon sink. Alternatively, the disruption of soil through agriculture and other land use has been suggested to account for

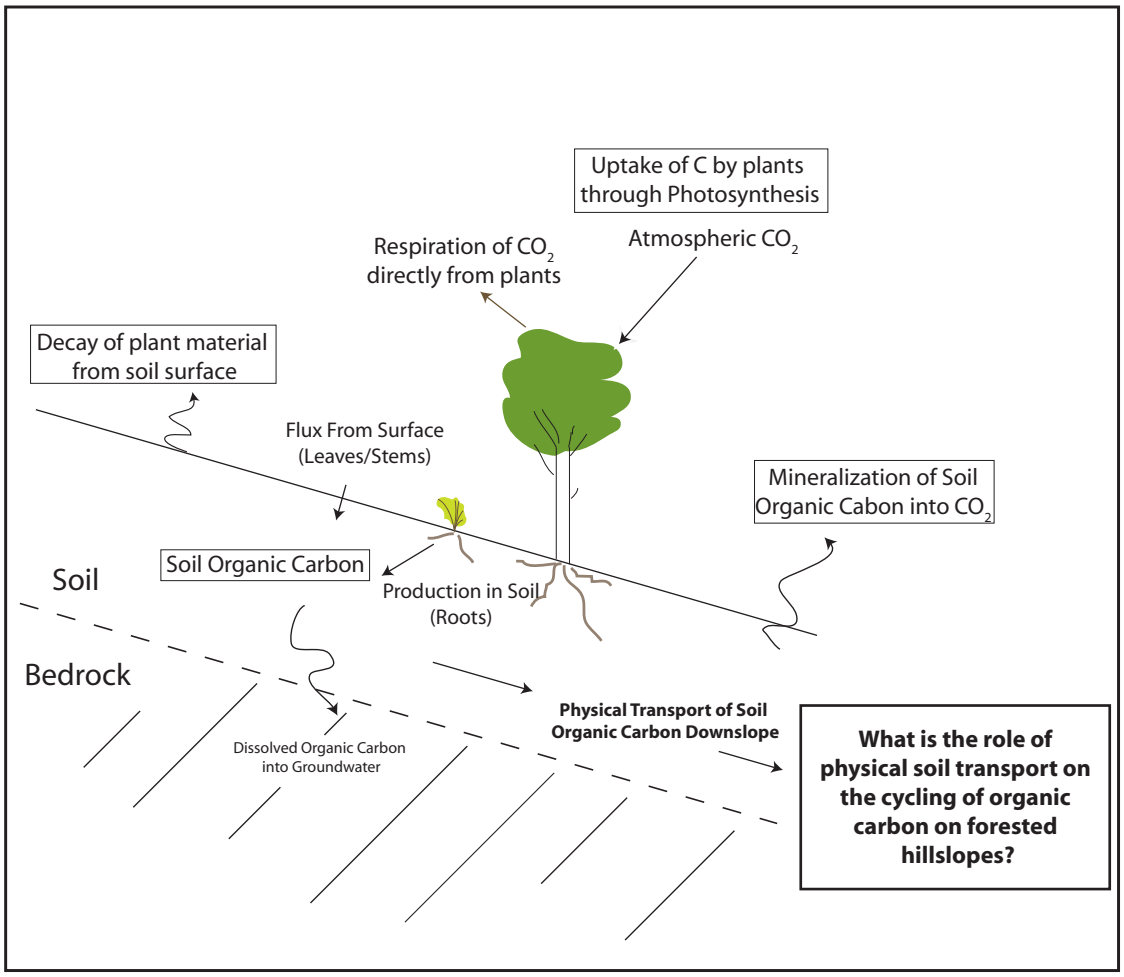

Figure 1. The carbon cycle on forested hillslopes. The focus of this study is on the role of physical soil transport and hillslope evolution on the cycling of organic carbon on forested hillslopes.

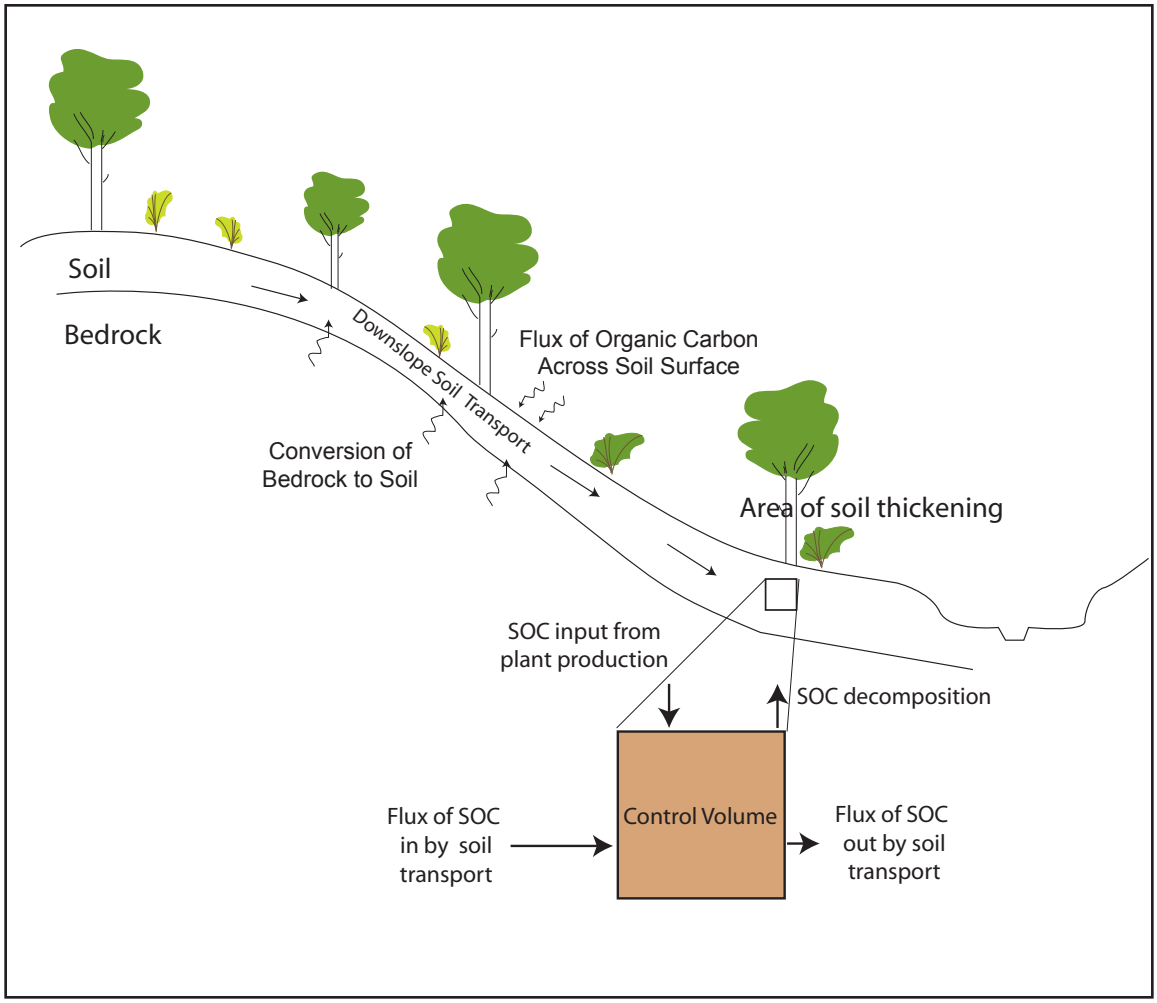

Figure 2. Conceptual model. This schematic diagram is of an idealized forested hillslope showing an area of soil thickening at the toe of the hillslope and the processes considered in the mass-balance model.

a possible atmospheric CO_2 source by increasing carbon mineralization of soil organic matter to CO_2 by biological decomposers (e.g. Lal, 2003, 2004). These types of studies are critical in discussions of the impact of land use changes on the global carbon cycle and identify the importance of soil transport in the cycling of organic carbon through soils, but these studies do not explore soil transport in natural environments. The role of soil transport on carbon cycling was recently investigated by Yoo et al. (2005, 2006) for undisturbed, grassy hillslopes in coastal California. The role of soil transport on carbon cycling for forested hillslopes has not been investigated.

The evolution of hillslopes dominated by slope-dependent soil creep processes has been shown to behave according to a diffusion-like equation (e.g. Culling, 1963; Carson and Kirkby, 1972; Nash, 1980; Fernandes and Dietrich, 1997). In the simplest form and neglecting tectonic motion, conservation of mass requires:

$$\frac{\partial}{\partial x} q_x + \frac{\partial \zeta}{\partial t} = 0, \tag{1}$$

where q_x [L^2 t^{-1}] is the volumetric flux density of soil in the x-direction per unit contour length, ζ [L] is land-surface elevation, t is time. Assuming the flux q_x satisfies the form,

$$q_x = -D \frac{\partial \zeta}{\partial x}, \tag{2}$$

where D [L^2 t^{-1}] is a diffusion-like coefficient, hillslope evolution can then be described by combining (1) and (2) such that:

$$\frac{\partial \zeta}{\partial t} = D \frac{\partial^2 \zeta}{\partial^2 x}. \tag{3}$$

Thus, the second derivative of land surface elevation, commonly referred to as hillslope curvature, determines whether hillslope soils are experiencing thickening (aggrading) or thinning (eroding). Soils thicken where the outgoing flux of soil from a control volume is less than the incoming flux, corresponding to positive hillslope curvature.

Areas of soil thickening create environments well suited for the preservation of organic carbon since: (1) there is a continual influx of organic carbon entrained in the soil, (2) the highest rates of soil transport and highest concentrations of organic carbon both occur near the soil surface, and (3) increasing soil depth (with thickening) reduces the rate of organic carbon mineralization to CO_2. Yoo et al. (2005) showed that organic carbon produced by roots *in situ* within thickened soils in depositional hollows accounted for much of the carbon stored on timescales of 10^3 to 10^4 years.

When there is a variation in soil thickness, soil transport depends on the depth of soil transport in addition to slope, the depth-slope product (Heimsath et al., 1999; Furbish and Fagherazzi, 2001; Furbish et al., 2009). Additionally, in locations of soil thickening, the mechanically active layer may not coincide with the depth to the soil-bedrock interface. It is therefore important to employ the depth-slope product to describe transport when studying locations of soil thickening.

The purpose of this study is to formally derive a fully depth-integrated mass-balance model utilizing a depth-slope product for the transport of soil organic carbon. Soil transport is coupled with biological organic carbon production and decomposition functions to explore the roles of these geomorphic and biologic processes on the cycling of organic carbon on forested hillslopes. The model is then compared to data collected in the field at the Land-Between-the-Lakes National Recreation Area of Tennessee.

CHAPTER II

THEORETICAL MASS-BALANCE MODEL

A vertically-integrated statement of conservation of mass for one-dimensional hillslope evolution is given by Furbish et al. (2009):

$$\frac{\partial}{\partial x}(h\overline{q_x}) + \frac{\partial}{\partial t}(h\bar{c}) + c(\eta)p(\eta) = 0, \tag{4}$$

where h [L] is the active soil thickness, c [$L^3 L^{-3}$] denotes the local volumetric concentration of soil particles per unit volume (c = 1 - porosity = ρ_s/ρ_r,where ρ_s and ρ_r are bulk density of soil and bedrock, respectively), p [$L\ t^{-1}$] is the rate of soil production, η [L] is the elevation of the soil base, and an overbar indicates depth averaging. The derivation of transport of soil organic carbon below follows the depth-integration of Mudd and Furbish (2004) and combines terms for the production and respiration of organic carbon.

Carbon mass is conserved starting with the following statement:

$$\nabla\cdot\mathbf{q}C + P_c - cCS_c + \frac{\partial cC}{\partial t} = 0, \tag{5}$$

where, with respect to a global reference frame, $\nabla = \mathbf{i}\partial/\partial x + \mathbf{j}\partial/\partial y + \mathbf{k}\partial/\partial z$, $\mathbf{q} = \mathbf{i}q_x + \mathbf{j}q_y + \mathbf{k}q_z$ [$L\ t^{-1}$] is the volumetric flux density associated with soil transports, C [$M\ L^{-3}$] is the mass fraction of organic carbon per volume of soil particles, P_c [$M\ L^{-3}\ t^{-1}$] denotes the rate of production of organic carbon within a unit volume, and S_c [t^{-1}] denotes the microbial respiration rate of organic carbon within a unit volume. Note that by multiplying the

volumetric concentration of soil c by the mass fraction of organic carbon C, the term cC represents the mass of organic carbon per unit volume. Similarly, the term $\mathbf{q}C$ represents the flux of organic carbon per unit area perpendicular to soil transport [M L^{-2} t^{-1}].

By considering two-dimensional soil transport in the x- and z-direction, the soil flux term $\nabla\cdot\mathbf{q}C$ can be expressed as

$$\nabla\cdot\mathbf{q}C = \frac{\partial q_x C}{\partial x} + \frac{\partial q_z C}{\partial z}. \tag{6}$$

Vertical integration of the soil transport terms above requires kinematic expressions for the local rates of change in the land surface ($z = \zeta$) and soil base ($z = \eta$), $\partial\zeta/\partial t$ and $\partial\eta/\partial t$. Note that the soil base does not necessarily coincide with the soil-bedrock interface, but rather where mechanical soil transport is zero.

A continuum "particle" identified with surface position ζ possesses the Langrangian coordinate x, which is a function of time. Independent of the x-coordinate, ζ may also vary with time. Thus,

$$\zeta = \zeta[x(t), t]. \tag{7}$$

Taking the derivitive of (7) with respect to time, $D\zeta/Dt$, obtains the total component of surface "particle" velocity parallel to z:

$$\frac{D\zeta}{Dt} = \frac{\partial\zeta}{\partial x}\frac{dx}{dt} + \frac{\partial\zeta}{\partial t}. \tag{8}$$

Evaluated at the land surface, $D\zeta/Dt = w(\zeta)$ and $dx/dt = u(\zeta)$, where $u(\zeta)$ and $w(\zeta)$ are components of the "particle" velocity parallel to x and z associated with soil motion at the surface independent of tectonic motion. Thus,

$$\frac{\partial \zeta}{\partial t} = w(\zeta) - u(\zeta)\frac{\partial \zeta}{\partial x} \tag{9}$$

The product $c(\zeta)w(\zeta)$ represents the flux density $q_z(\zeta)$ associated with soil motion at the land surface at any instant. Likewise, $c(\zeta)u(\zeta) = q_x(\zeta)$. Multiplying each term in (9) by $c(\zeta)$ and $C(\zeta)$, the mass flux of organic carbon at the surfaces gives:

$$\frac{\partial \zeta}{\partial t} c(\zeta) C(\zeta) = q_z C(\zeta) - q_x C(\zeta)\frac{\partial \zeta}{\partial x} + I_\zeta \tag{10}$$

where I_ζ [$ML^{-2}t^{-1}$]denotes the flux of organic carbon across the land surface ζ into the soil through the mechanical disturbance of the soil surface and overlying organic matter.

By definition, the flux of soil at the base of the active soil layer, $q_x(\eta) = q_z(\eta) = 0$. The vertical motion of the base of the active soil layer, $\partial\eta/\partial t$, may be nonzero. Neglecting vertical tectonic motion:

$$\frac{\partial \eta}{\partial t} = p_\eta \tag{11}$$

where p_η denotes the local rate of change in η due to soil production.

Vertical integration of the soil flux term q_x associated with the first term in equation (5) between the limits $z = \zeta$ and $z = \eta$ using Lebniz's rule gives:

$$\int_\eta^\zeta \frac{\partial q_x C}{\partial x} dz = \frac{\partial}{\partial x}\int_\eta^\zeta q_x C dz - q_x(\zeta) C(\zeta)\frac{\partial \zeta}{\partial x} + q_x(\eta) C(\eta)\frac{\partial \eta}{\partial x}. \tag{12}$$

Integration of the soil flux term q_z associated with the first term in equation (5) gives:

$$\int_\eta^\zeta \frac{\partial q_z C}{\partial z} dz = q_z(\zeta) C(\zeta) - q_z(\eta) C(\eta). \tag{13}$$

Integration of the fourth term in equation (5) using Leibniz's rule gives:

$$\int_{\eta}^{\zeta} \frac{\partial cC}{\partial t} dz = \frac{\partial}{\partial t} \int_{\eta}^{\zeta} cCdz - c(\zeta)C(\zeta)\frac{\partial \zeta}{\partial t} + c(\eta)C(\eta)\frac{\partial \eta}{\partial t}. \tag{14}$$

Collecting (11) through (14) and regrouping, and recalling that $q_x(\eta) = q_z(\eta) = 0$:

$$\frac{\partial}{\partial x} \int_{\eta}^{\zeta} q_x Cdz - q_x(\zeta)C(\zeta)\frac{\partial \zeta}{\partial x} + q_z(\zeta)C(\zeta) + I_{\zeta}$$

$$+ \frac{\partial}{\partial t} \int_{\eta}^{\zeta} cCdz - c(\zeta)C(\zeta)\frac{\partial \zeta}{\partial t} + c(\eta)C(\eta)\frac{\partial \eta}{\partial t} = 0. \tag{15}$$

Making use of our simplified kinematic expressions (11) and (12), equation (15) can be simplified to:

$$\frac{\partial}{\partial x} \int_{\eta}^{\zeta} q_x Cdz + \frac{\partial}{\partial t} \int_{\eta}^{\zeta} cCdz + c(\eta)C(\eta)p_{\eta} + I_{\zeta} = 0. \tag{16}$$

Evaluation of the integrals in (16) using the mean value theorem then leads to

$$\frac{\partial}{\partial x}(h\overline{q_x C}) + \frac{\partial}{\partial t}(h\overline{cC}) + c(\eta)C(\eta)p(\eta) + I_{\zeta} = 0, \tag{17}$$

where $h = \zeta - \eta$ is the active soil thickness and an overbar denotes a vertically averaged quantity. Equation (17) describes mechanical downslope transport of soil organic carbon together with source terms for the flux of organic carbon across the upper and lower soil surfaces.

The two terms in equation (5) dealing with biogenic production and decomposition of organic carbon (P_c and S_c, respectively) may be vertically integrated in the same way as the soil transport terms, such that:

$$\int_{\eta}^{\zeta} cCS_c = h\overline{cCS_c}. \tag{19}$$

$$\int_{\eta}^{\zeta} P_c = h\overline{P_c} \tag{18}$$

Expressions for the organic carbon input and decomposition rates are adapted from Yoo et al. (2005), and exponentially decrease with soil depth:

$$P_c = P_0 e^{-\psi/\alpha} \tag{20}$$

$$\mathrm{S_c} = \mathrm{S_0} e^{-\psi/\beta} \tag{21}$$

where the subscript 0 represents the surface production and decomposition rates, $\psi = \zeta - z$ denotes the depth from the surface, and α and β represent *e*-folding depths where the soil *C* input and decomposition rates, respectively, are equal to 1/*e* of the surface values.

Combining the vertically integrated organic carbon production and decomposition terms with the vertically integrated soil transport terms gives:

$$\frac{\partial}{\partial x}(h\overline{q_x C}) + \frac{\partial}{\partial t}(h\overline{cC}) + c(\eta)C(\eta)p(\eta) + I_\zeta + \overline{P_c} - \bar{c}\overline{CS_c} = 0. \tag{22}$$

The flux of soil is assumed as a depth-slope product (Ahnert, 1967; Furbish and Fagherazzi, 2001; Anderson, 2002; Heimsath et al. 2005) , such that:

$$q_x = -D^* h \frac{\partial \zeta}{\partial x}, \tag{23}$$

where D^* [L t^{-1}] is a diffusion like coefficient.

The soil production function (Heimsath et al., 1997) is:

$$p(\eta) = -p_0 e^{h/\gamma}, \tag{23}$$

where p_0 [L t^{-1}] is the initial soil production rate for fresh bedrock and γ [L] is the *e*-folding depth of soil production.

This model shows that the change in soil organic carbon storage is a function of transport of organic carbon in or out of a control volume, the flux of organic carbon across the soil surface, the incorporation of any organic carbon at the soil base, production of organic carbon within the soil, and respiration of organic carbon within the soil. Equation (22) is the basis of modeling (Chapter IV) for comparison with field data.

To numerically solve equations (4) and (22), I use explicit finite differencing (involving central differencing) and incorporate the algebraic expressions into MatLab code to solve the two equations simultaneously, choosing appropriate time steps to keep the model stable. In the MatLab code, equation (22) was altered to distinguish between the mechanically active layer and the depth to the soil-bedrock interface, which becomes important in areas of soil-thickening. Model results were compared to topographic data and to calculated soil organic carbon storage values from field samples to explore the role of different model parameters on the cycling of organic carbon on hillslopes. MatLab code used in the modeling is given in Appendix B.

CHAPTER III

METHODS

Field Site

The field site selected to compare with modeling results is in the Panther Creek watershed at Land-Between-the-Lakes National Recreation Area. Land-Between-the-Lakes (LBL) is bound to the east and west by reservoirs on the Cumberland and Tennessee rivers, respectively, creating a 15-20 km wide strip of land running north-south from Tennessee into Kentucky (Figure 3). Base level for the Cumberland and Tennessee rivers is the Ohio River 30 km north of the canal connecting Lake Barkley (Cumberland River) and Kentucky Lake (Tennessee River) at the northern boundary of LBL. Observation of map and digital elevation models suggest that incision of the Ohio River has propagated upstream to tributaries of the Cumberland and Tennessee rivers, which are actively downcutting into the flat Mississippian karst plain of the interior low plateau to form slopes up to 30°. LBL is situated in a humid temperate climate. Mean annual precipitation is 1210 mm. Average temperatures are 3°C in winter and 28°C in summer (Franklin et al., 1993).

Hillslopes flanking the lowest order tributaries of watersheds directly adjacent to the Cumberland and Tennessee Rivers merge into flat, undisected uplands at the hillslope crest. These hillslopes in the low-order watershed are considered to be at earlier stages of hillslope evolution relative to those flanking higher order tributaries. For this study, three hillslopes were selected that represent hillslopes of different "ages" or at different stages

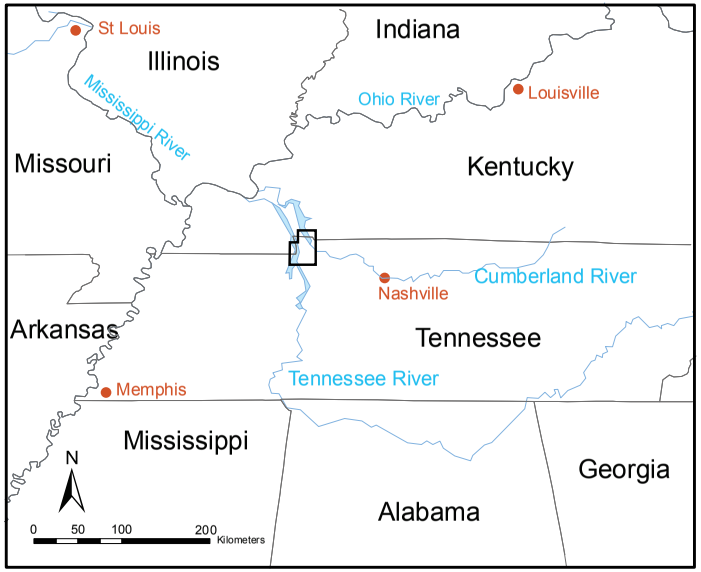

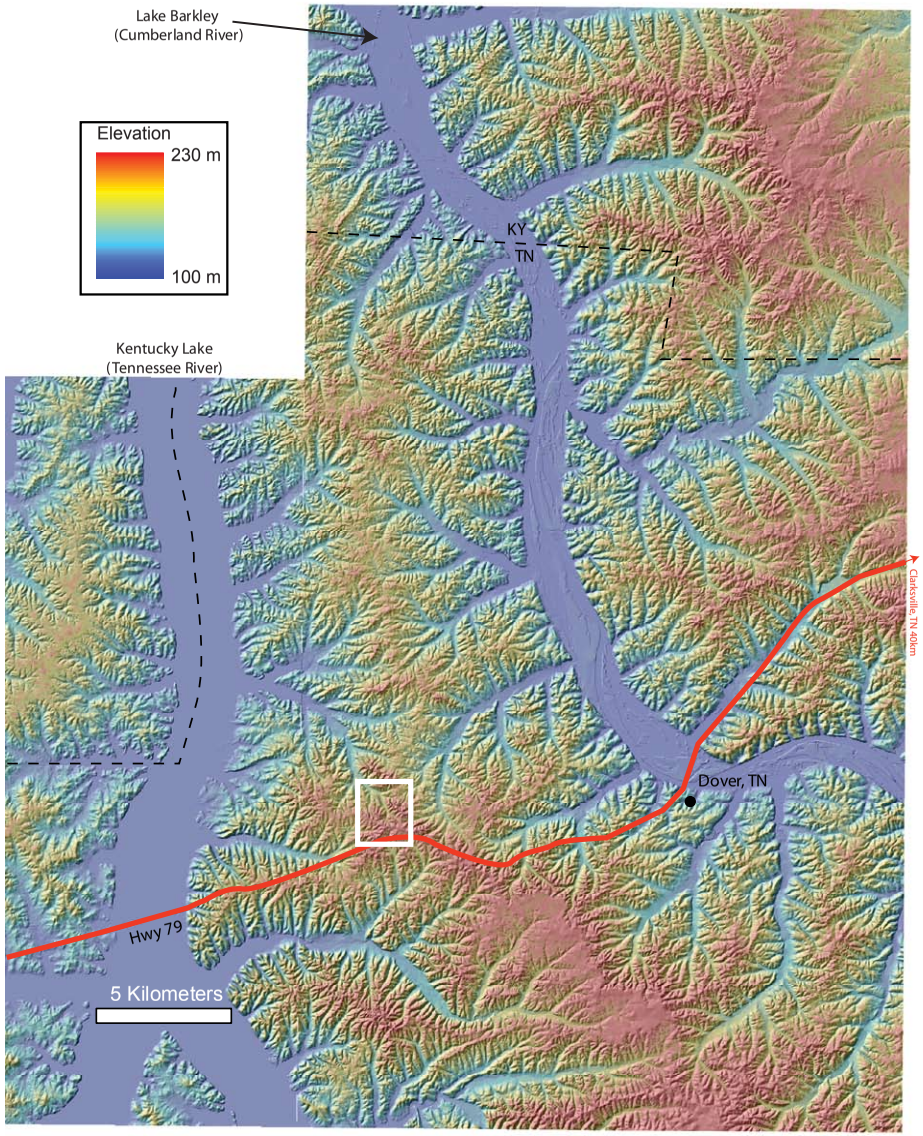

Figure 3. Location map and digital elevation model (DEM) of the field area. The 10m resolution DEM is underlain by hillshade relief with 2x vertical exaggeration. Notice that slope is significantly lower in areas farthest away from the Cumberland and Tennessee Rivers, e.g. the northwest and south-central portions of the DEM. The white box is the outline of the contour map in Figure 8 showing the study sites.

of evolution along the same ridgeline in the upper Panther Creek watershed, all vegetated with oak-hickory forest. These locations are named the Upper, Middle, and Lower hillslopes. The Upper hillslope, immediately adjacent to an intermittent first-order stream, represents the earliest stage of evolution relative to the other two locations. The Middle hillslope is separated from a seasonal second-order stream by a poorly define terrace/floodplain. The Lower hillslope, representing the latest stages of evolution relative to the other two locations, is separated from a seasonal third-order stream by a well defined terrace.

The lithology of the Panther Creek watershed is mainly comprised of the Mississippian Fort Payne, Warsaw, and St. Louis Formations (Marcher, 1965). The Warsaw and St. Louis Formations are both fossiliferous limestones with abundant, but discontinuous, chert layers. The Fort Payne Formation consists of chert intercalated with highly siliceous limestone. Hillslopes of the three field sites are formed on the Warsaw and St. Louis limestones with Fort Payne underlying the under-fit stream valleys filled with chert-rich stream gravel. Hillslopes in the lower elevations of the Panther Creek watershed, closer to the outlet of Panther Creek to Kentucky Lake/Tennessee River, are formed on the Fort Payne Formation. The higher elevations, above approximately 190 m and mostly along the flat, undisected drainage divides in southern LBL, are capped with the Cretaceous Tuscaloosa Gravel consisting of subrounded chert clasts in a sandy clay matrix. The extent of Tuscaloosa Gravel in the Panther Creek watershed is considerably less significant than the Fort Payne, Warsaw, and St. Louis Formations. Tuscaloosa Gravel and small amounts of Pleistocene loess may exist in small, discontinuous, unmapped deposits in the Panther Creek watershed (Harris, 1988).

Soils mantling the Mississippian limestone formations in the upper Panther Creek watershed consist of residual silt, clays and chert that accumulate as the limestone chemically weathers (Larson and Barnes, 1965). The concentration of iron nodules in LBL soils supported mining operations during the 1800s. Larson and Barnes (1965) report that the residuum of the Warsaw and St. Louis formations were not excavated in the Standing Rock quadrangle, in which the upper Panther Creek watershed resides. There are no active or abandoned soil pits or gravel pits mapped within the watershed (Marcher, 1965 and 1967).

It is important to note, that although Panther Creek is now considered a pristine stream, historical land use has affected the watershed. Nearly all of the LBL area was logged at least once to fuel iron smelting operations, most of which ceased shortly after the end of the Civil War in 1865. Although I have not been able to find an accurate historical account of land use in the Panther Creek watershed, it is estimated that most of LBL was reforested between 80-100 years ago (Franklin et al., 1993).

Topographic Surveying

One-dimensional transects were surveyed at the Upper, Middle and Lower hillslopes. Locations of the transects were carefully selected to be perpendicular to topographic contours and free of any major topographic variations from uprooted trees or local oversteepening by stream undercutting. Surveying was completed with a Sokkia B20 optical transit. Elevations along the slopes were measured relative to benchmarks placed at the crest of the hillslopes. Each transect ends in the stream channel. Transects for the Middle and Lower hillslope are roughly perpendicular to the stream as these

locations occur along a linear ridge running parallel to the valley. Because the Upper hillslope is still responding to active incision, the surveyed transect is at an acute angle to the stream in the upstream direction. Detailed directions to the field area and GPS locations of hillslope benchmarks are given in Appendix C.

The second derivative of land surface elevation is commonly referred to as hillslope curvature in the geomorphologic literature. Slopes with negative curvature are convex up; those with positive curvature are concave up. Hillslope curvature for the irregularly spaced topographic survey data is approximated by taking the difference in the slopes about a point and dividing by one-half the total change in horizontal distance (figure 4). Calculating hillslope curvature from survey transect data is important in determining locations where hillslope soils are likely eroding (convex up) and likely aggrading (concave up).

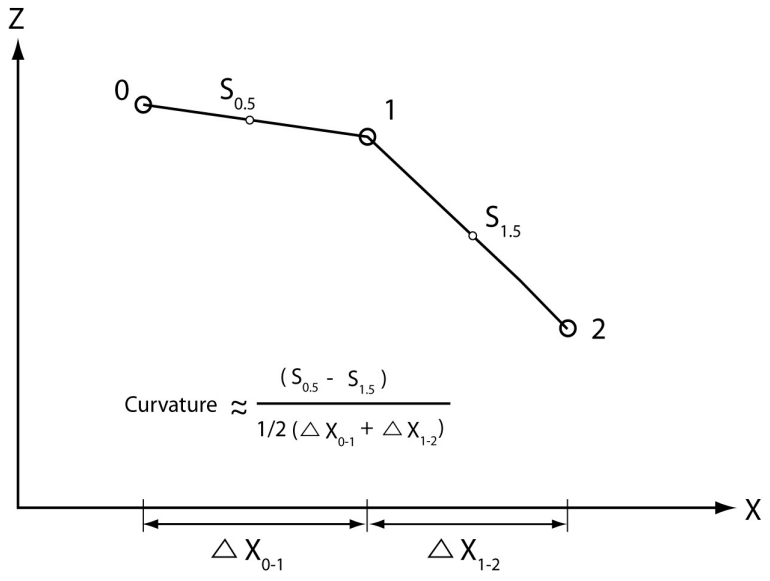

Figure 4. Calculation of hillslope curvature for irregularly spaced data. S is the average slope between survey points.

Soil Pits and Sampling

A total of 15 soil pits were dug along the three surveyed transects to sample soils at various depths. Soil pit locations were measured relative to known positions along the transects and were spaced along the transect such that the features of the hillslope morphology were represented in the sampling (e.g. at the hillslope crest, where curvature is negative, positive or changes, at the hillslope toe). The maximum depth we were able to dig determined the total depth of individual soil pits. Because of extreme hardness of the B-horizon in the summer months, when all but one soil pit was dug, the final depths of pits were above the soil-bedrock interface. Digging pits was easier in winter when soils had higher moisture, but the quick infilling of the pit with water inhibited reaching the soil-bedrock interface.

Aluminum cylinders were used to sample soil volume in order to calculate bulk density. Cylinders measure 5 cm in diameter and were 5-6 cm in length. Sampling cylinders were hammered into the vertical pit wall with a cloth covering the exposed end to inhibit soil from falling out of the cylinder. Once the sampling cylinder was even with the pit wall, the cylinder was dug out and the excess soil was sliced away such that the volume of soil in the sampling cylinder represented the undisturbed volume of soil. Soil used for bulk density measurements were also analyzed for organic carbon. Where high pebble or root concentrations prevented accurate sampling with cylinders, soil material was collected for organic carbon analysis only. Sampling intervals increase from 5 cm intervals (the diameter of cylinders) in the upper 30-40 cm of the soil to 10-15 cm intervals well below the A-horizon. The uppermost sample in the soil profile was taken by hammering the cylinder from the soil surface down into the soil. Leaf and twig litter

was removed before digging pits and sampling on the surface. A thin, 1-2 cm layer O-horizon was removed when taking a surface sample.

The infiltration capacity of the soil at four locations on the Middle hillslope was measured to determine the likelihood of surface flow versus groundwater flow paths for precipitation. An infiltration ring 15 cm in diameter was placed into the soil at the surface and at one location on the top of the B-horizon. Care was taken to minimize disturbance of the soil. Known volumes of water were poured into the ring, whence the duration of time it took for the water to reach the soil surface was measured. This process was repeated until the duration of time to drain the volume was the same between applications, representing the steady state infiltration rate.

Sample Processing and Analysis

All soil samples collected from pits were weighed and then placed in an oven to dry. Oven temperature was kept low (<60ºC) so that organic matter would not oxidize. Samples were dried until sample masses were unchanged after additional time in the oven. Soil bulk density (g cm^{-3}) was calculated by dividing the total dry sample mass by the volume of the cylinder used in sampling. Because organic carbon is confined to the soil material, samples were sieved to 2 mm and the mass of the >2 mm fraction was measured. The mass of the >2 mm fraction is used in soil organic carbon calculations discussed below.

The <2 mm soil fraction was used in organic carbon analysis. Approximately 10 g of the <2 mm soil fraction was crushed with a mortar and pestle for analysis on a Perkin Elmer 2400 Series II CHN (Carbon, Hydrogen, Nitrogen) Analyzer at the Hancock

Biological Station operated by Murray State University, Murray, Kentucky. From the crushed sample, 1-2 mg of sample was used in the CHN analyzer. The sample was weighed to 0.001 mg. Digestion with sulfuric acid removed inorganic carbon from samples prior to CHN analysis. Calibration of the CHN analyzer was performed with known standards and a conditioning agent under the direction of Hancock Biological Station staff. In addition to soil, roots from within a soil profile and organic matter from the thin O-horizon were analyzed for CHN.

Output of the CHN analyzer used in this study are carbon (organic) and nitrogen percentages (mass fraction multiplied by 100) and molar carbon-to-nitrogen (C:N) ratios. Soil organic carbon storage refers to the mass of organic carbon per square meter of soil surface. The storage for each soil pit to a depth of 50 cm was calculated by summing the soil organic carbon storage at intervals of 0-5cm, 5-15cm, 15-30cm, and 30-50cm. Soil organic carbon storage, *S*, at any interval, *i,* is calculated by:

$$S_i = h_i \rho_i (1 - R_i) C_i, \tag{23}$$

where h_i [L] is the interval thickness, ρ_i [M L^{-3}] is the interval-averaged soil bulk density, R_i [M M^{-1}] is the interval-average mass fraction of rocks greater than 2 mm, and C_i [M M^{-1}] is the average mass fraction of organic carbon for the interval.

Photographs of the crushed CHN samples document variation in color of soils at different depths and positions on hillslope. Photographs were taken with a Zeiss AxioCam MRc 5 camera on a Zeiss Stemi 2000-C stereo microscope. Photographs for all but one soil pit (09JR01) were taken with the same camera settings in one session to allow for cross-comparison of soil pits and hillslopes.

CHAPTER IV

RESULTS

Field Results

To model soil transport on hillslopes as a diffusive-like process, the potential for soil erosion by overland flow must be considered. Minimum infiltration rates from infiltration tests on the Middle hillslope represent the precipitation intensities needed to produce overland flow at the study site. The lowest infiltration rates of tests done on the soil surface were 0.02 cm s^{-1} (Figure 5), equating to a precipitation intensity of approximately 70 cm hr^{-1}. Minimum infiltration rates of 0.005 cm s^{-1} for the B-horizon were significantly lower than on the soil surface, corresponding to a precipitation intensity on the order of 10 cm hr^{-1}. As discussed below, this implies that overland flow at LBL is rare enough that soil transport is considered to be diffusive-like.

There is no field evidence, e.g. rills, gullying, or accumulation of organic matter, behind surface bumps, at the study area to suggest that overland flow is responsible for soil transport on the hillslopes. Tree throw was observed at several locations in the study area (Figure 6). Large worms, up to 15 cm in length and 1.5 cm in diameter, were found in soil pits at the lower elevations of the Middle and Lower hillslopes where soil remains moist during the summer months relative to positions higher on the hillslope (Figure 7). Worms and corresponding tubes were found well into the B-horizon. The occurrence of small burrowing mammals, mainly moles and shrews, at LBL is noted by (Feldhamer et

al., 2002) but their occurrence is limited in the uplands. No evidence for burrowing mammals was observed at the field site during this study.

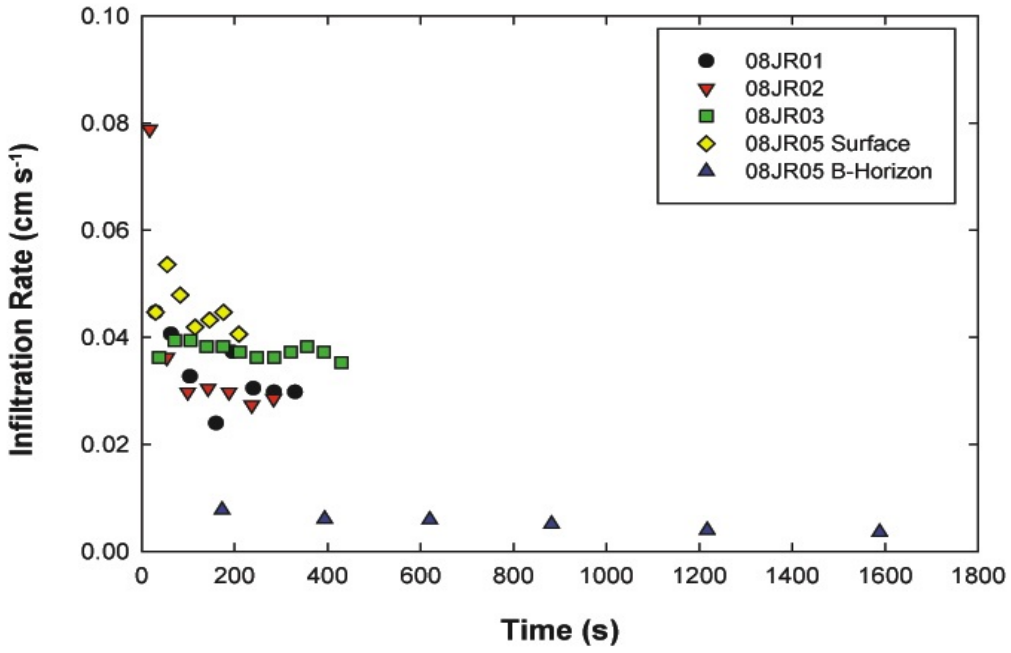

Figure 5. Infiltration rates measured at the Middle hillslope using a single-ring infiltrometer.

Surveyed transects of the three hillslopes reveal that hillslope morphology is dependent on the relationship of the hillslope to the stream (Figure 8). The convex up morphology of the Upper hillslope is due to the actively incising stream immediately adjacent to the hillslope base. The Middle and Lower hillslopes, separated from active fluvial processes by a valley flanked with small terraces, are convex up at the hillslope crest and concave at the base. These two hillslopes have inflection points, where curvature changes from negative to positive, at approximately 40 m and 50m, respectively (Figure 9).

Figure 6. Photographs of tree throw at LBL. Numerous instances of tree throw were observed at the field area. Photo on the left is of a pine tree at the service road used to enter the park, overturned during a January, 2009 ice storm.

Figure 7. Photographs of a worm and worm tube from soil pit 08JR05 on Middle hillslope. The pocket knife is 8 cm in lengh.

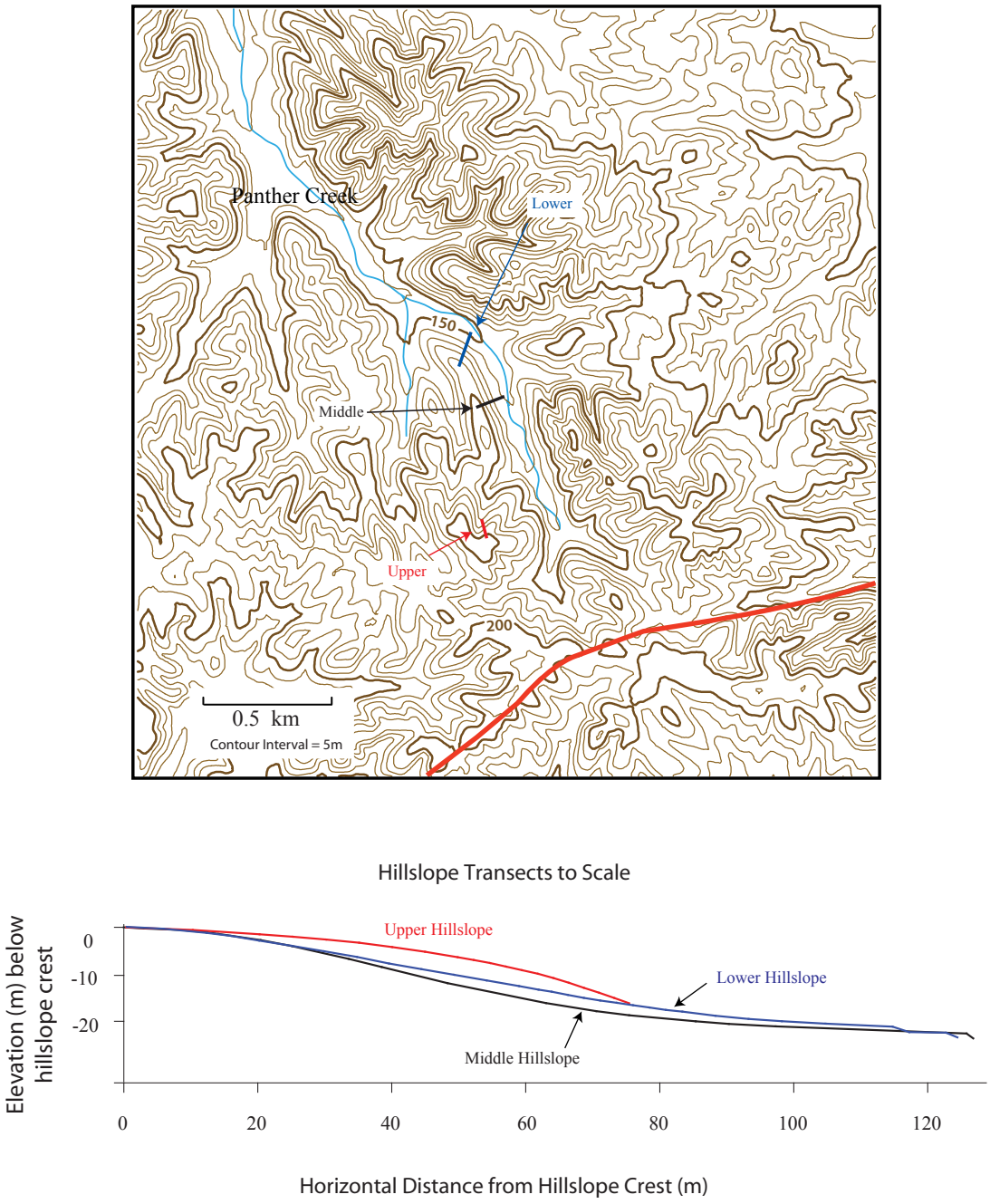

Figure 8. Location of survey transects (top) and transects plotted to scale (bottom). Contour map (top) was created from a 10 m DEM to show the relationship of hillslope transects to each other and the topography of the Panther Creek watershed. Land surface elevation (bottom) from survey data shows that the Upper hillslope has convex up morphology, while the Middle and Lower hillslopes have convex-concave morphology.

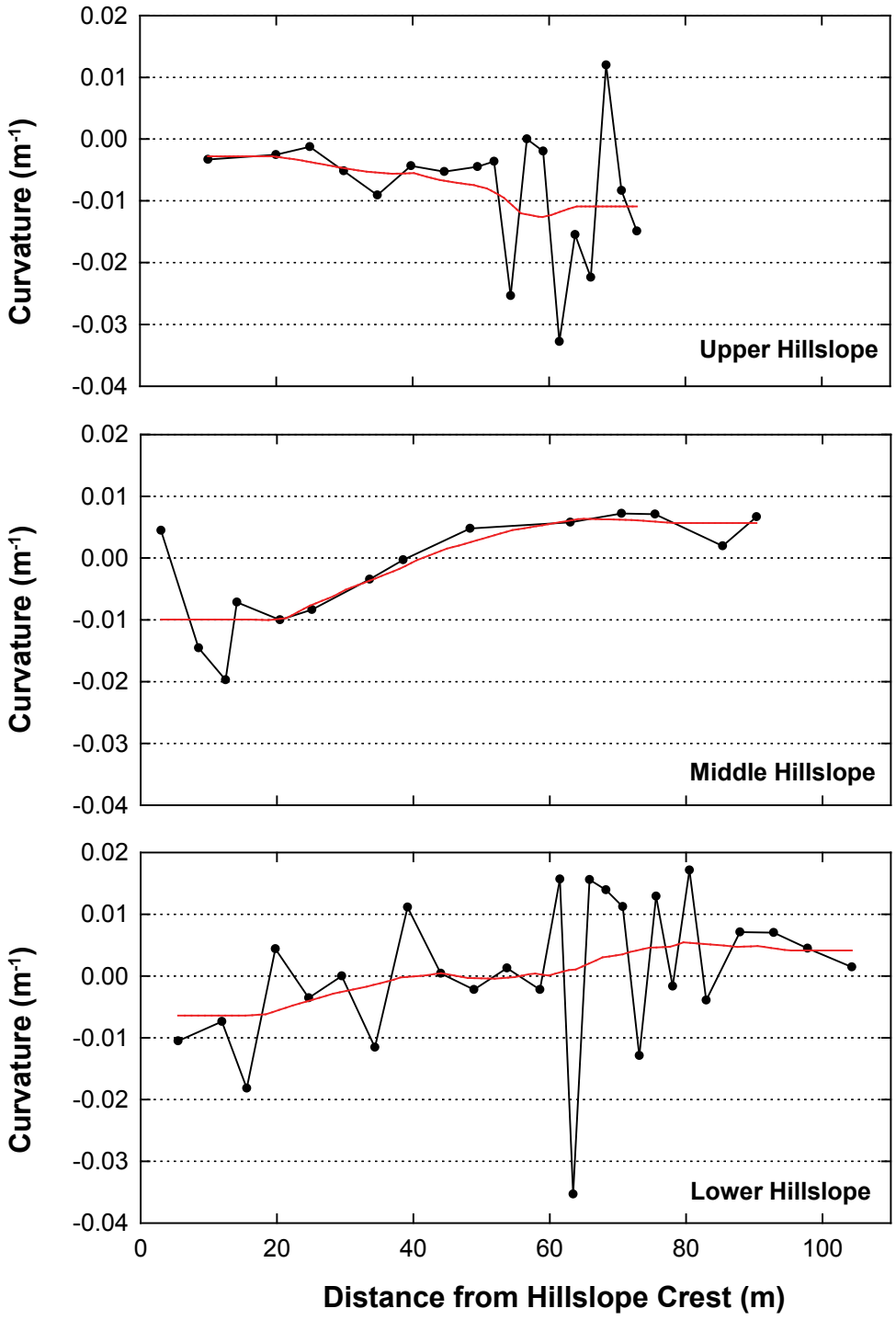

Figure 9. Hillslope curvature of the Upper, Middle and Lower hillslopes (black line with points). Hillslope curvature is also plotted with a 5 point moving average (red line) to smooth variability caused by surface roughness. Note that, when smoothed, the Upper hillslope has negative curvature for the entire transect, while the Middle and Lower hillslopes have curvature inflection points at approximately 40 and 50 m, respectively.

The nature of the fluvial terrace system of Panther Creek is important in understanding landscape and hillslope evolution of the study area, but a detailed investigation of the complex fluvial system is beyond the scope of this study. The convex-concave morphology of the Middle and Lower hillslopes is seen throughout the watershed at places where hillslopes are separated from the stream by a terrace or floodplain. At some locations in the Panther Creek watershed the stream has migrated across the valley and is actively undercutting and oversteepening hillslopes. Any soil stored at the toe of the hillslope on a terrace surface is removed at locations where hillslopes are oversteepened and terraces are eroded by the stream. The hillslope-terrace interface is an ideal location to store transported hillslope soil and organic carbon within the watershed. The Middle and Lower hillslopes, both at locations with a broad terrace, were selected for this reason.

The mass fraction of clasts greater than 2 mm in soil samples was highest in soil pits on the Middle and Upper hillslopes (Figure 10). Plots for the upper hillslope do not accurately represent the high occurrence of rocks in soil pits because of the high number of samples taken without bulk density sampling cores. The majority of clasts greater than 2 mm are residual rounded chert and quartzite from the Cretaceous Tuscaloosa Gravel. Fragments of the underlying limestone and angular chert from nodules from within the limestone comprised a small fraction of the >2 mm clasts and are generally smaller than the rounded gravel clasts. A thin lag of Tuscaloosa Gravel is exposed on the soil surface at the crest of the Upper hillslope transect and is present throughout all soil pits dug into this hillslope. A small topographic high on the ridgeline just south of the Middle hillslope

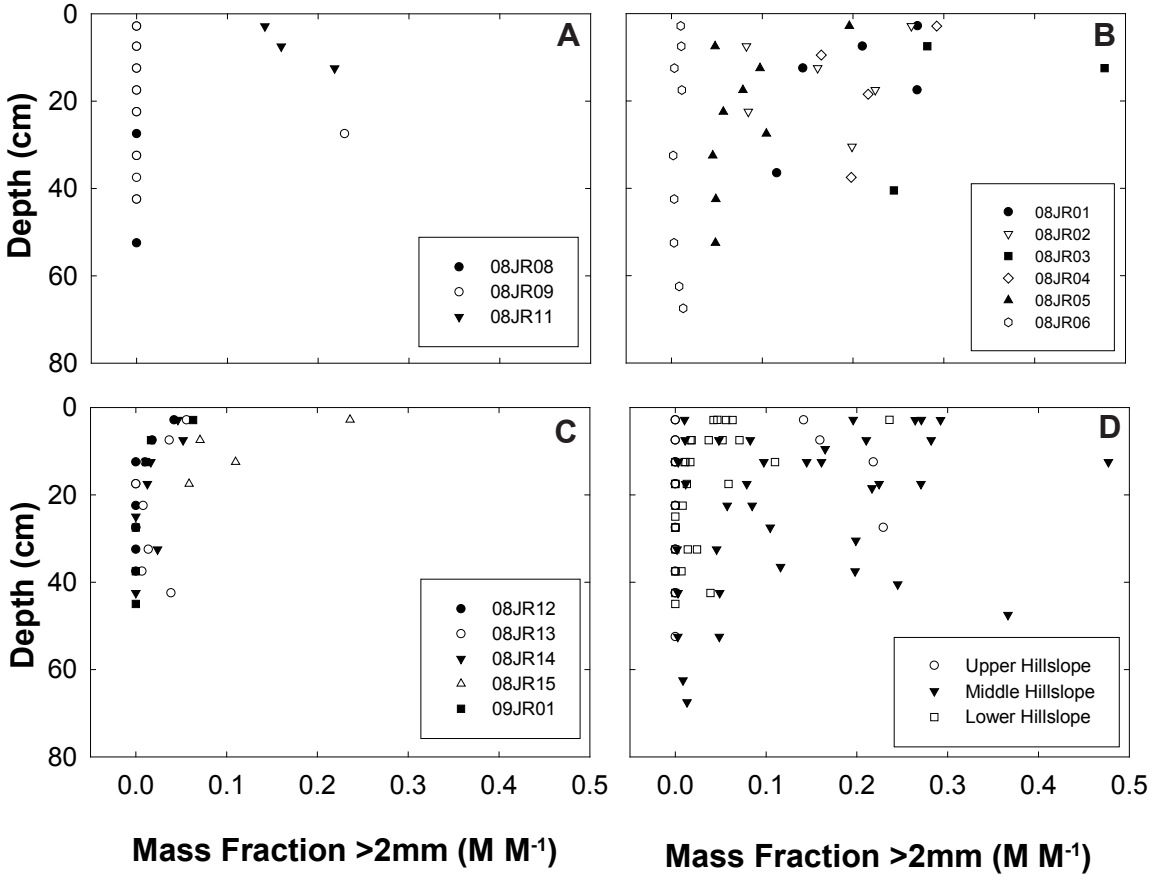

Figure 10. Plots of the mass fraction of clasts >2 mm from soil samples for the Upper (A), Middle (B), and Lower (C) hillslopes, and all samples combined (D).

also exhibits a surficial lag of gravel. The gravel lag is thought to hold up the small topographic high south of the Upper hillslope crest benchmark.

To determine if soil mixing processes responsible for soil transport are dependent on hillslope position, soil bulk density for soil pits at the three hillslopes were plotted against depth. Although bulk density generally increases with depth, there is no systematic variation in bulk density with respect to position on the hillslope (Figure 11), suggesting that the frequency of disturbances is relatively uniform over the entire hillslope. Likewise, the similarity in bulk density among the three hillslopes suggests relative uniformity in the frequence of soil disturbances over the three hillslopes.

Comparing photographs of soil samples qualitatively shows a thickening of the A-horizon at the toe of the hillslope relative to the crest (Figures 12-14). Soils are darker at deeper intervals in soil pits at the toe of the hillslope. Soil organic carbon percentages rapidly decrease from 2-5% at the surface to generally 1% or less below a depth of 15 cm. Soil organic carbon percentages vary little between soil pits and hillslopes below ~15 cm depth. Samples 08JR03-F and 08JR05-G, both on the Middle hillslope, have anomalously high SOC percentages for their depths. There is little difference in soil organic carbon concentrations among the three hillslopes (Figures 12-14, and15).

Organic carbon-to-nitrogen (C:N) ratios are plotted versus depth for the Upper and Middle hillslopes (Figure 16). The Lower hillslope was omitted because nitrogen values are extremely low. Maximum C:N ratios of 10-20 occur at the soil surface, and this ratio quickly decreases with depth. The Middle hillslopes exhibits higher C:N ratios than the Upper hillslope, especially in depths below 10 cm. Plotting C:N ratio versus percent soil organic carbon shows that C:N ratio is dependent primarily on carbon

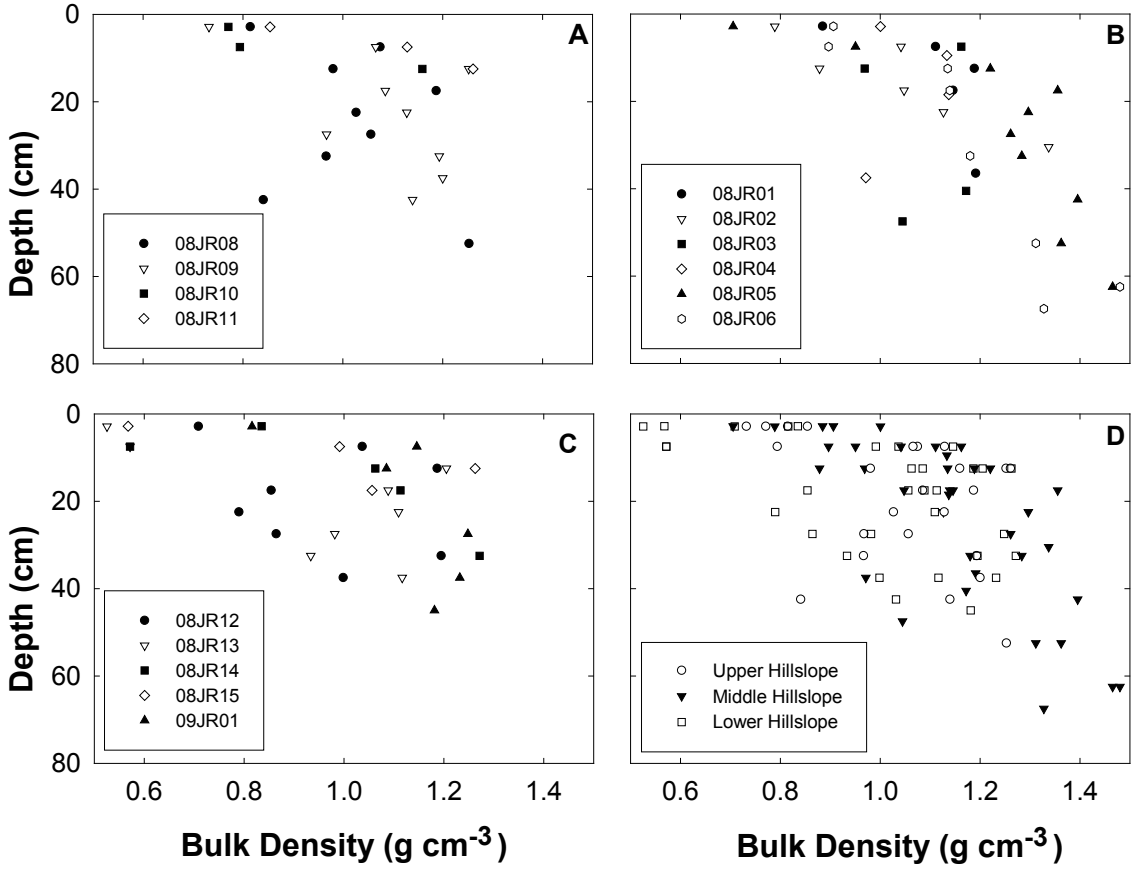

Figure 11. Plots of soil bulk density versus depth for the Upper (A), Middle (B), and Lower (C) hillslopes, and all samples combined (D).

concentrations. Nitrogen concentrations are low and there is a general decrease in nitrogen with depth (Figure 16).

The O-horizon at 09JR01 and root material from 08JR12 were analyzed on the CHN as references for initial %C and C:N values of organic carbon enter into or produced within the soil. The organic matter from 09JR01 has 40% organic carbon and 27.4 C:N ratio, while the roots from 08JR12 has 47% organic carbon and 24.6 C:N (Appendix A). The C:N ratios for O-horizon and roots are on the same order as surface soil samples, but the percent carbon is significantly higher than soil organic carbon values.

The soil organic carbon storage at each interval was calculated for all soil pits (figure 17). Soil organic carbon storage is sensitive to variations in bulk density and percent soil organic carbon. Although SOC storage is generally highest at the 0-5 cm depth, there is greater variability of SOC storage with depth. The 30-50 cm interval for 08JR05 on the Middle hillslope has the highest SOC storage value due to high bulk density and an anomalously high percent of organic carbon in sample 08JR05-G at 30-35 cm. Comparing depth integrated SOC storage down to 50 cm depth for soil pits shows the total mass of organic carbon has a weakly positive correlation to curvature and distance from the hillslope crest (figure 18).

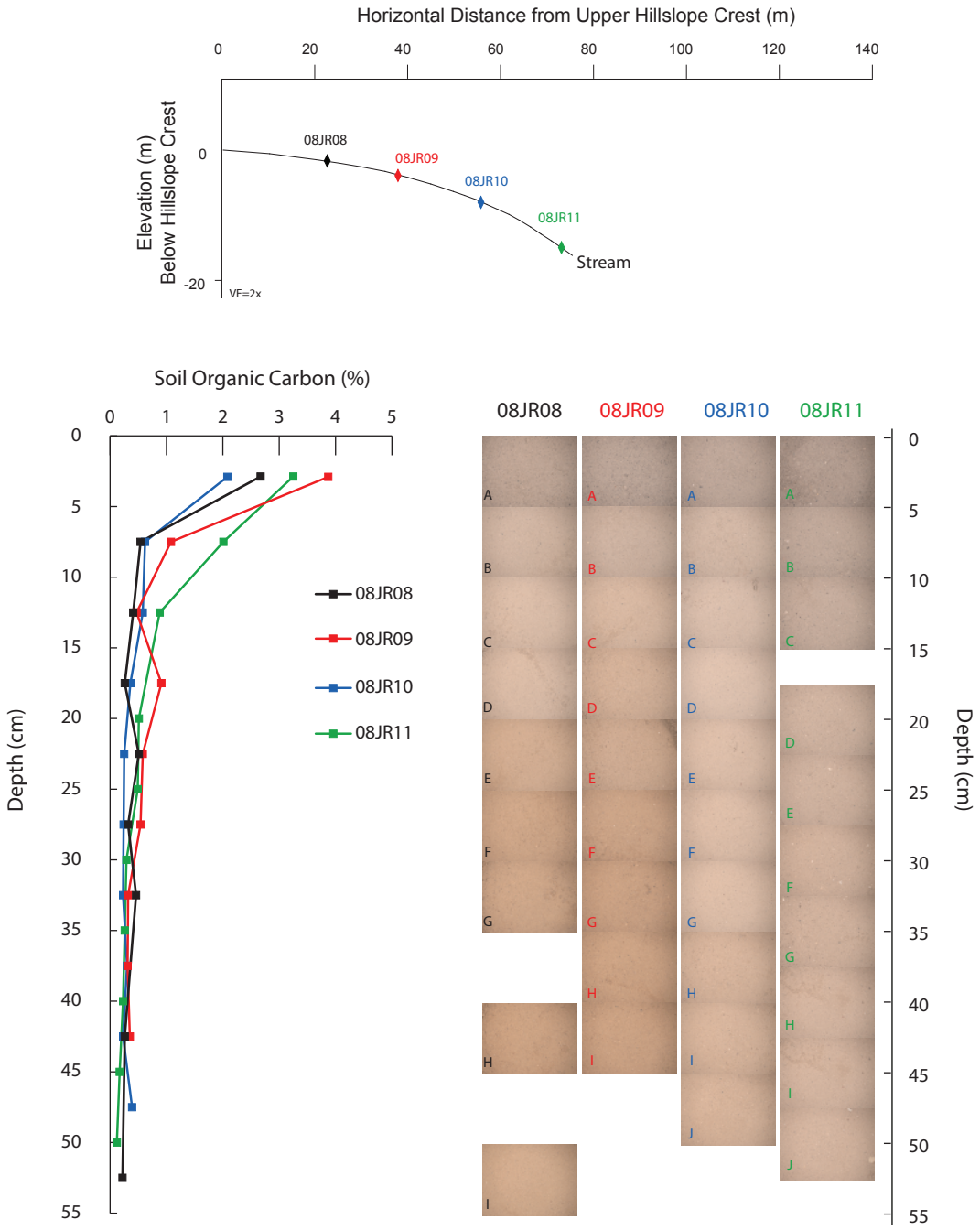

Figure 12. Location of soil pits plotted on transect survey (above), photographs of soil samples (right), and plot of percent soil organic carbon versus depth (left) for the Upper hillslope.

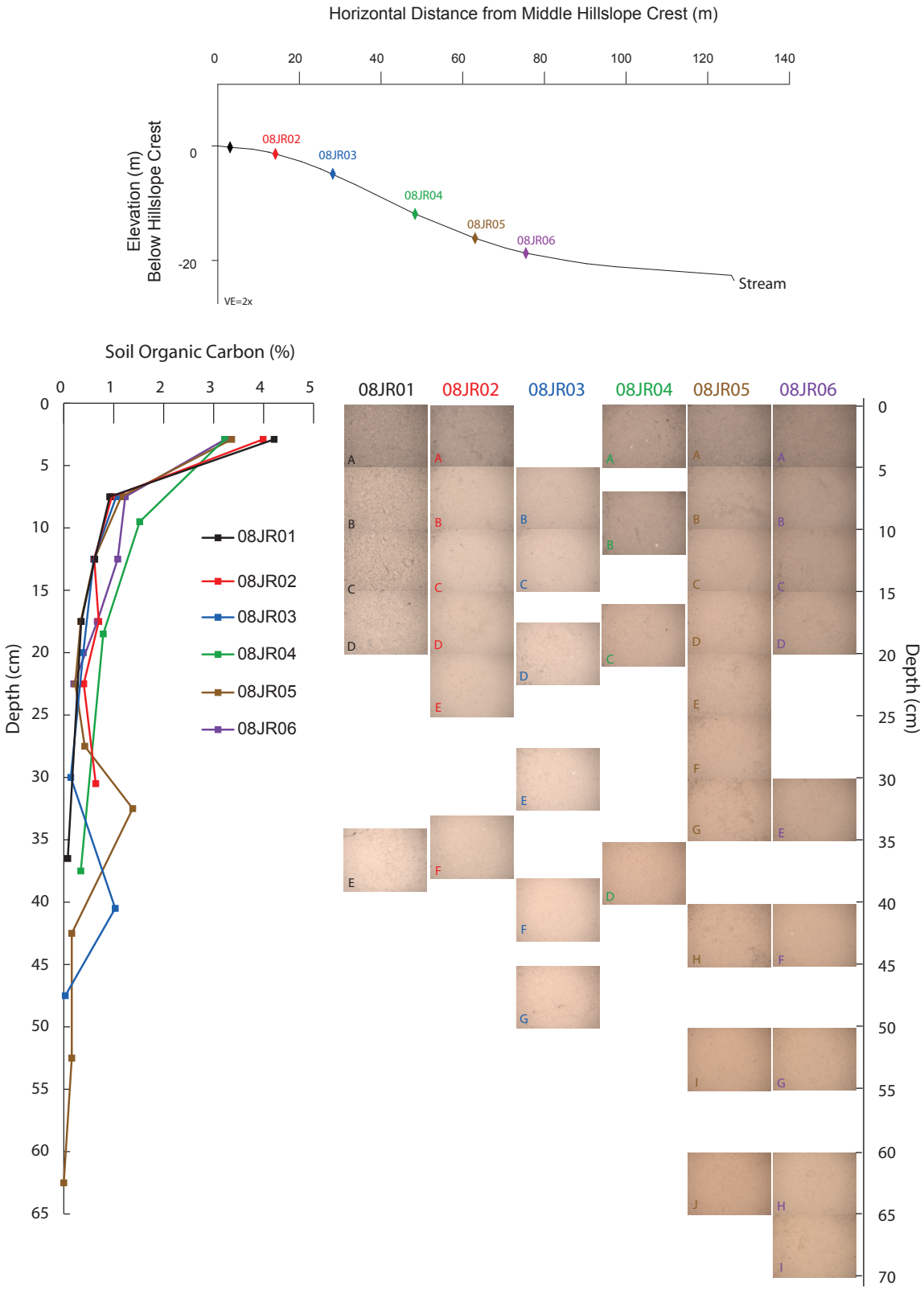

Figure 13. Location of soil pits plotted on transect survey (above), photographs of soil samples (right), and plot of percent soil organic carbon versus depth (left) for the Middle hillslope.

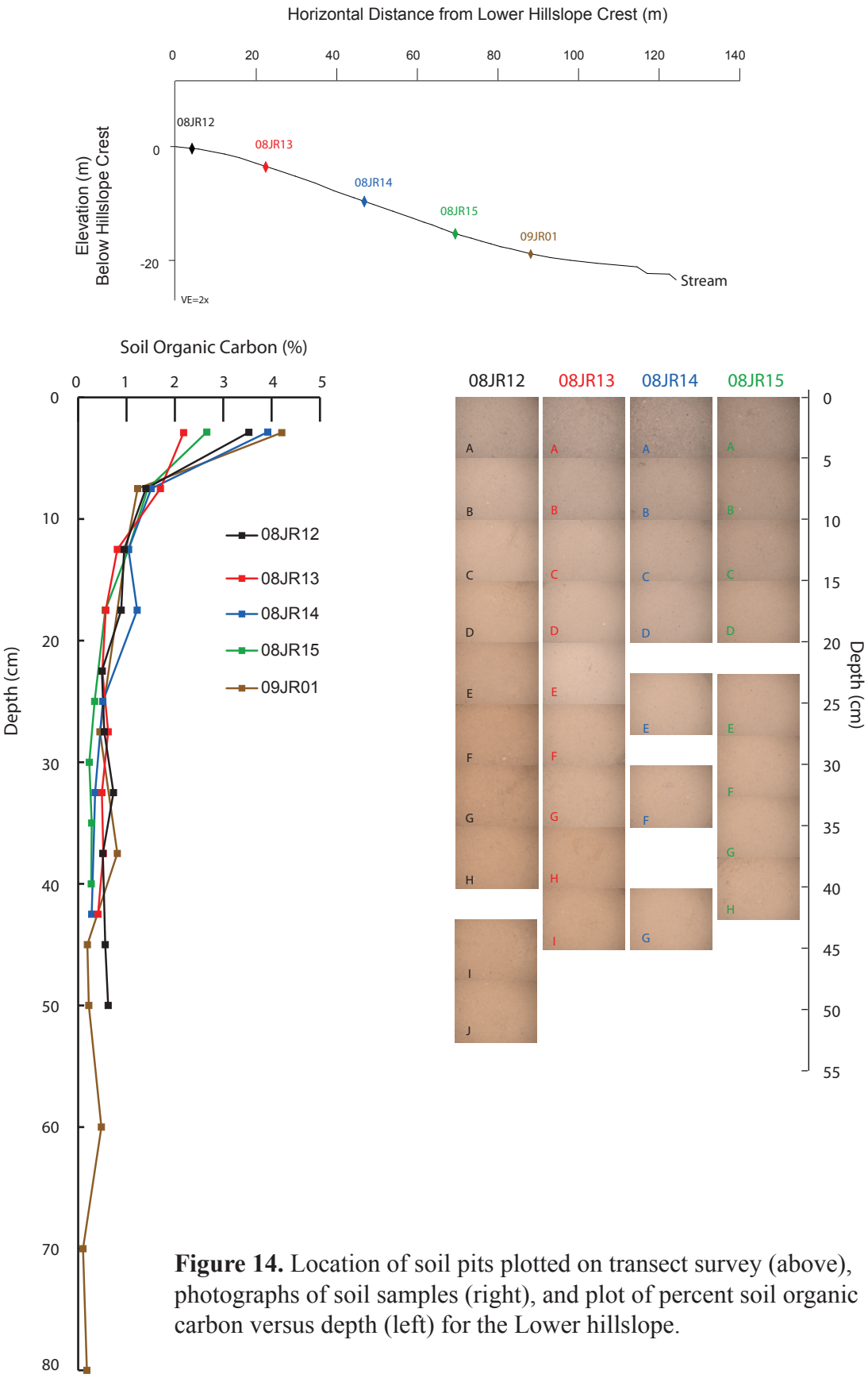

Figure 14. Location of soil pits plotted on transect survey (above), photographs of soil samples (right), and plot of percent soil organic carbon versus depth (left) for the Lower hillslope.

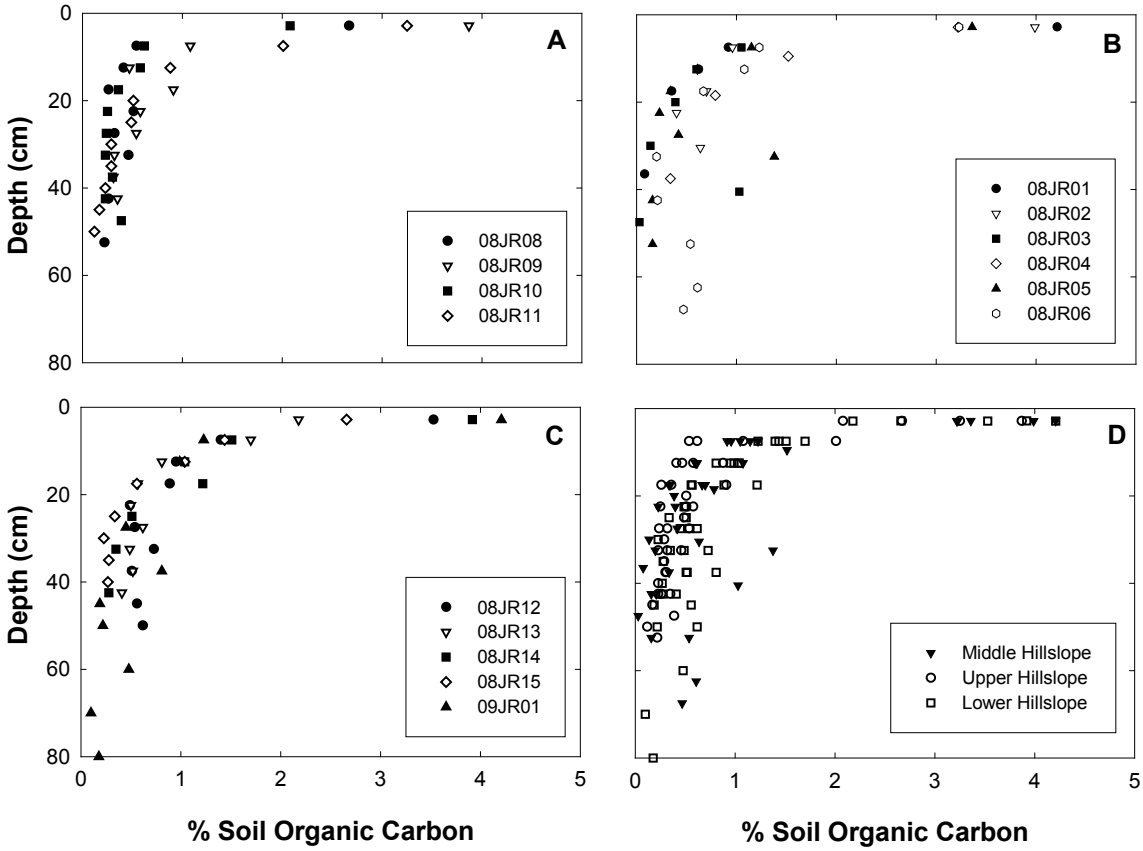

Figure 15. Plots of percent soil organic carbon versus depth for the Upper (A), Middle (B), and Lower (C) hillslopes, and all samples combined (D).

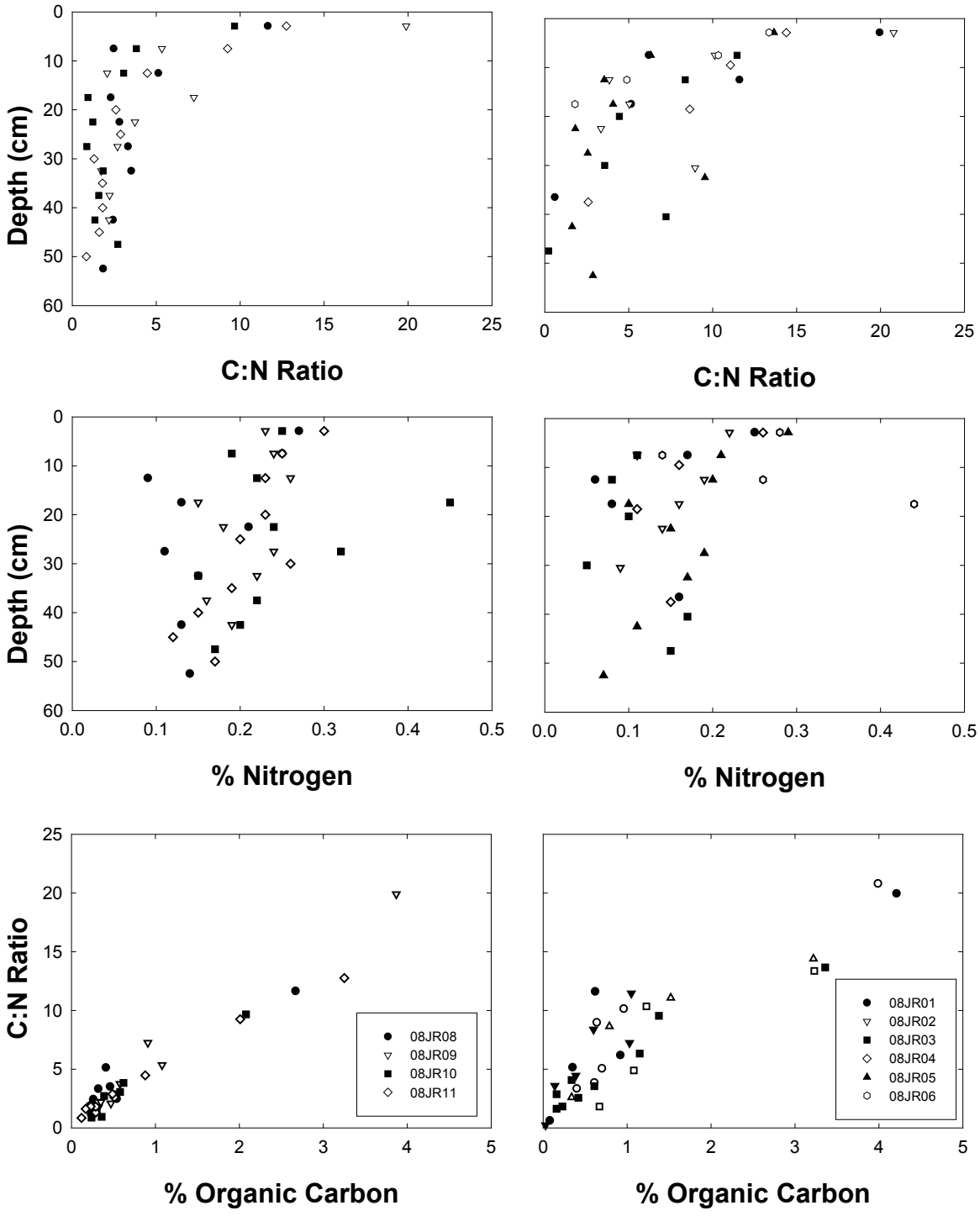

Figure 16. Plots of C:N ratio versus depth (top), percent nitrogen versus depth (middle), and percent organic carbon versus C:N ration (bottom) for the Upper (left) and Middle (right) hillslopes. Because there is only a slight decrease in nitrogen with depth, C:N ratios are mostly dependent on % organic carbon.

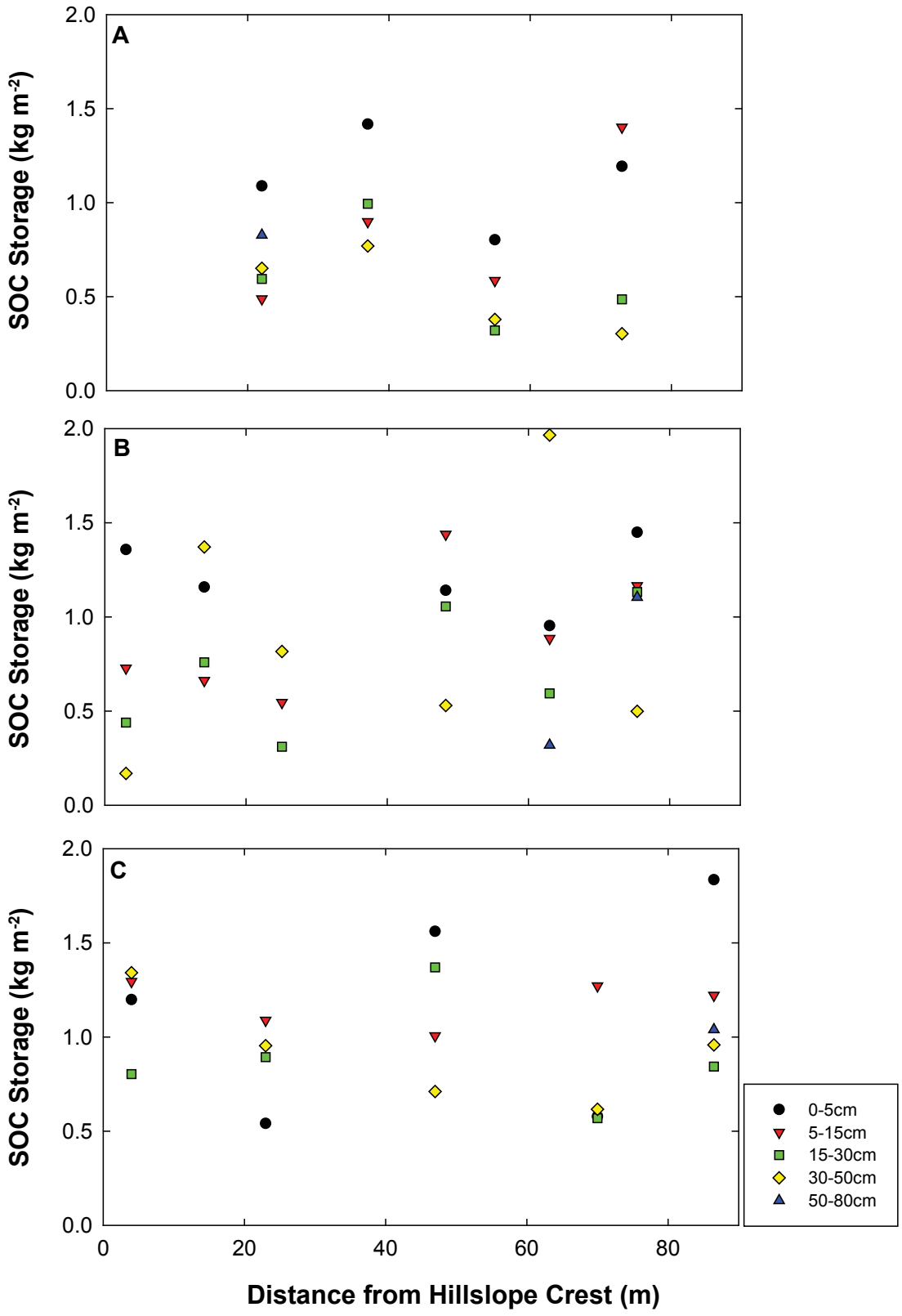

Figure 17. Plots of soil organic carbon storage versus depth at sampled intervals versus distance from hillslope crest for the Upper (A), Middle (B), and Lower (C), hillslopes.

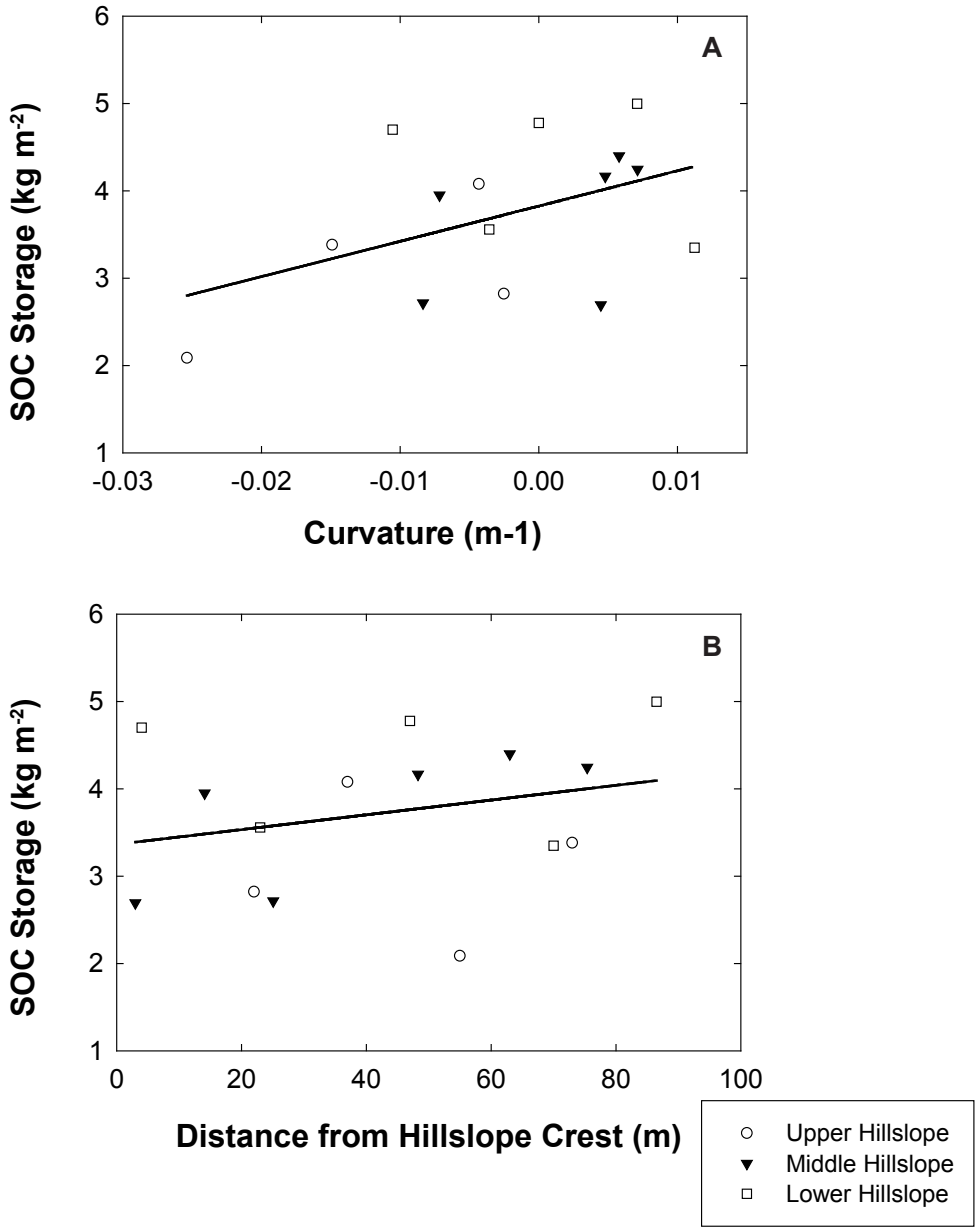

Figure 18. Plot of soil organic carbon storage versus hillslope curvature (A) and distance from hillslope crest (B). SOC storage shows a weak positive trend with curvature and distance from crest. Lines are linear regressions with $R^2 = 0.2$ (A) and 0.45 (B).

Modeling Results

Model Parameterization

Field data were used where possible to parameterize the soil organic carbon storage model. Although the scope of the field investigation makes it difficult to accurately determine many of the parameters, values in the model are within an order of magnitude of those typically seen in the literature. It is important to note that modeling is geared toward gaining insight into how different parameters influence the system and the physical interpretation of processes influencing carbon storage.

The high infiltration capacity of soils at the field area indicates that soil transport by overland flow is not likely significant. Minimum infiltration rates measured at the Middle hillslope provide a conservative estimate of a 10 cm hr^{-1} precipitation intensity to produce overland flow. The average recurrence interval at nearby Dover, TN for a 10 cm hr^{-1} precipitation event sustained for 30 minutes is 25 years and for 60 minutes is 500 years (NOAA, 2004; Figure 19). Furthermore, the absence at the field area of features indicative of overland flow agrees with the infiltration data that overland flow is likely rare. Soil transport can therefore be modeled diffusively. A combination of root growth, worm and insect burrowing, tree throw, and to a lesser extent expansion and contraction of clays, are likely the dominant soil transport mechanisms.

These types of soil transport mechanisms are reflected in the variability of bulk density measurements. The disruption of soil by tree throw likely accounts for the greatest amount of variability in bulk density because tree throw is more widely spaced and occurs on a more infrequent time scale than burrowing. Much of the localized surface roughness

on hillslopes is attributed to remnants of tree throw. The variability in bulk density represents a snapshot of the balance between soil lofting resulting from mechanical soil disturbances and the loss of the porosity by particle settling (Furbish et al., 2009). By time averaging these dilations and contractions, the depth averaged-bulk density, and thus the depth-averaged volumetric concentration of soil particles, are assumed to remain constant through time. The depth-averaged volumetric concentration of soil particles over the interval ζ to η is 0.5 and at η is 0.7 for all model simulations.

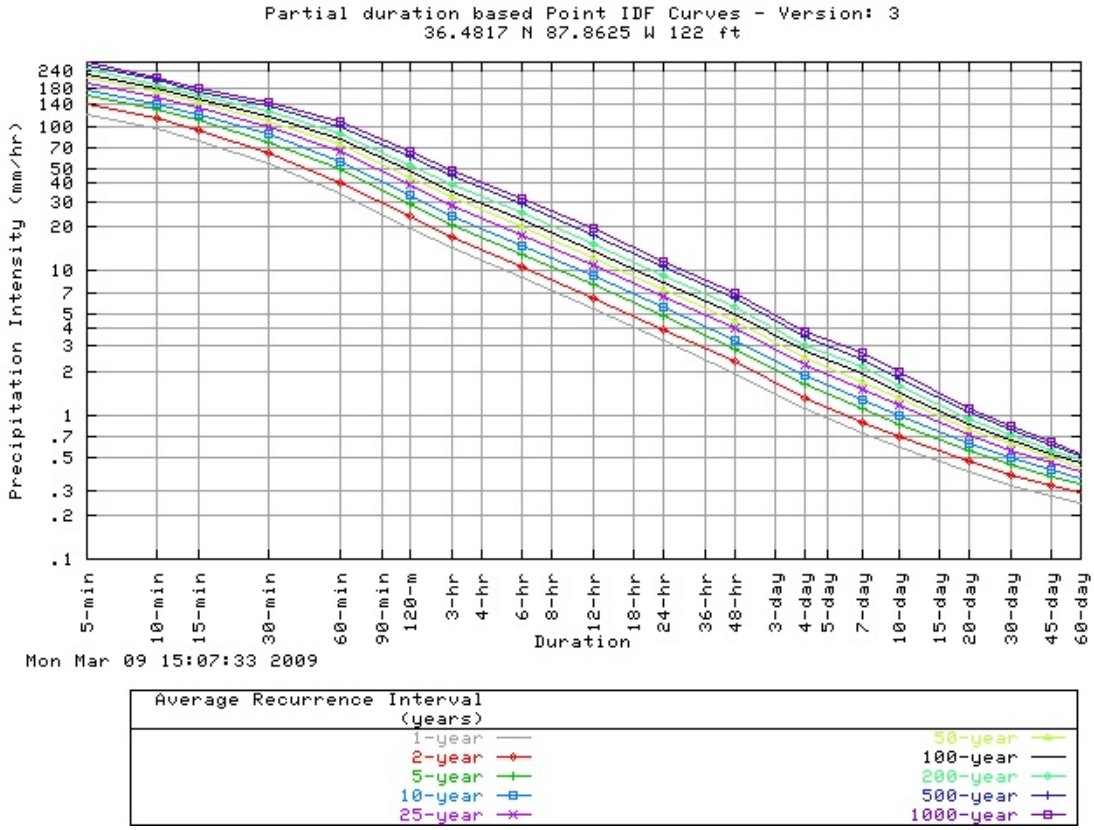

Figure 19. Intensity-duration-frequency curves for Dover, Tennessee (NOAA, 2004). The conservative estimate for precipitation intensity necessary to create surface flow at LBL is on the order of 10 cm hr^{-1}. Precipitation events sustained at that intensity for 60 minutes occur every 500 years on average.

Although the greatest concentrations of roots are found in the upper 20-30 cm of the soil profiles, roots were present as deep as 80cm, indicating that soil transport is active to at least that depth and possibly deeper. Where measurements extend below a depth of 50 cm (Figure 11 D) bulk density appears to level off, indicating a decreasing frequency of mechanical disturbances with depth. A maximum soil transport depth on the order of 1 m is reasonable based on soil pit observations and bulk density measurements.

The rapid decrease in percent soil organic carbon and C:N ratios with depth is interpreted as resulting from organic carbon experiencing significant decomposition before soil mixing can move a large portion of the carbon incorporated into the soil at the surface to depths greater than 10-15cm. Additionally, the production of biomass in soils is highest near the surface. The C:N ratios for roots and organic matter at the field site are similar to surface C:N ratios of soil organic carbon. In more thoroughly mixed soils, C:N ratios are more homogenous with respect to depth. For example, pocket gopher burrowing in coastal California (Yoo et al. 2005, 2006) and surface wash in Colorado steppe (Schimel et al., 1985) both resulted in soils with C:N ratios between 8-13 at the surface decreasing to a minimum of 6 as deep as 250 cm.

Furthermore, soil C:N ratios in the upper 10 cm fall within the range of C:N ratios typical of fungi (10-15), that generally feed on “fresh” organic material in aerated forest soil (Paul, 2007). Bacteria, on the other hand, typically have C:N ratios of 3.5-7 and are able to live in a wider range of soil environments than fungi (Paul, 2007). C:N ratios measured between 10-20 cm are within the range of those given for bacteria. Most samples below a depth of 20 cm have C:N ratios less than 3.5:1, except for a few soil pits on the Middle hillslope that have higher C:N ratios.

The incision and aggradation history for the Green River, central Kentucky, a tributary of the Ohio River, was determined over the past 3.5 million years (Ma) from cosmogenic nuclides in Mammoth Cave sediments by Granger et al. (2001). Periods of Green River infilling and incision correspond to major advances and retreats of ice sheets within the Ohio River basin. Incision occurred rapidly, with rates of ~30 m Ma^{-1} in the Pleistocene. The most recent aggradation occurred at 0.7-0.8 Ma ago. Presently, there are 10 m of sediment in the Green River valley that formed behind Ohio River valley sediment trains in the Wisconsinan. A similar incision and aggradation history is expected for the Tennessee and Cumberland Rivers and their tributaries. The broad, under-fit valleys at the study area possibly resulted from rapid incision and infilling associated with glacial perturbations. Although the exact chronology of incision and aggradation for the study area is not known, the work done on the Green River provides a framework for making assumptions about the relationship between hillslope and fluvial systems in the Panther Creek watershed.

The formation of soil on terraces at the toe of hillslopes is modeled as occurring instantaneously and with the same initial conditions as the hillslope. This is reasonable given that the invasion of vegetation onto unconsolidated terrace sediment and soil formation occur far more quickly than the timescale of hillslope evolution. The purpose of modeling in this study is to understand the influence of hillslope processes on organic carbon cycling, not the details of landscape evolution for the study area.

Initial Conditions

Six different model simulations are discussed here. Of these simulations, five represent hillslope relaxation with a terrace at the hillslope toe and one represents hillslope evolution following incision of a flat surface. Elevation data from the Upper hillslope transect was used as the initial condition for land surface in the five simulations of hillslope relaxation. Roughness in land surface for the initial condition results in perturbations in the soil organic carbon storage that becomes smoothed out as time progresses (Figure 20). The amount of time to smooth these perturbations depends on the initial soil production rate and the diffusion coefficient; however, the effects of these perturbations are typically minimized within 10 thousand years (ka) or less.

The initial value for soil organic carbon storage is somewhat arbitrary as equilibrium between organic carbon input and respiration is reached in less than 100 years (Figure 20), insignificant compared to the timescale of hillslope evolution and soil transport. Soil organic carbon storage was initially set at 5 kg C m^{-2} for the five hillslope relaxation simulations and 4 kg C m^{-2} for the incision simulation. These initial soil organic carbon storage values were chosen because they are close to the equilibrium reached shortly after the simulation begins. Initial soil thickness for all simulations is 1 m.

Flux of Organic Carbon Across the Soil Surface

The flux of organic carbon across the soil surface interface results from mechanical disturbances at the soil surface. At LBL and in most forested areas, there is a year round cover of litter on the soil surface. A balance between leaf fall, decomposition of leaves on the soil surface, and incorporation of biomass into the soil occurs such that

the amount of leaf litter remains essentially constant through time. Therefore, the thickness (or mass) of yearly leaf fall on the soil surface does not limit the amount of carbon entering the soil but instead is limited by the soil mixing rate on the surface. Exploring the influence of this term on soil organic carbon storage reveals a shift in the total amount of soil organic carbon storage (Figure 21). For all the simulations discussed here, the flux of carbon across the surface (I_{ς}) was kept at 0.1 (kg m^{-2} t^{-1}) for consistency among simulations.

Overall Trends in Hillslope Relaxation Simulations

The general trend observed in simulations of hillslopes relaxing onto terrace surfaces is for soil organic carbon storage to increase with distance from the hillslope crest, with an abrupt increase in soil organic carbon storage where soils thicken at the hillslope toe. As time progresses from 10 ka to 100 ka, the inflection point from negative to positive hillslope curvatures shifts toward the crest. Likewise, the location where soils begin to thicken follows the same trend. Although there is significant thickening of soils in the downslope direction from the peak soil thickness, the increase in organic carbon associated with this thickening is minimal. The decrease in slope on the downslope side of peak soil thickness decreases the soil transport rate, allowing more organic carbon to decompose before burial. The low slope causes soils deposited on the terrace surface to not exceed a maximum value that represents equilibrium between organic carbon inputs and decomposition. It is in the upslope migration of the thickening soil environment where the potential is created to significantly increase soil organic carbon storage through time.

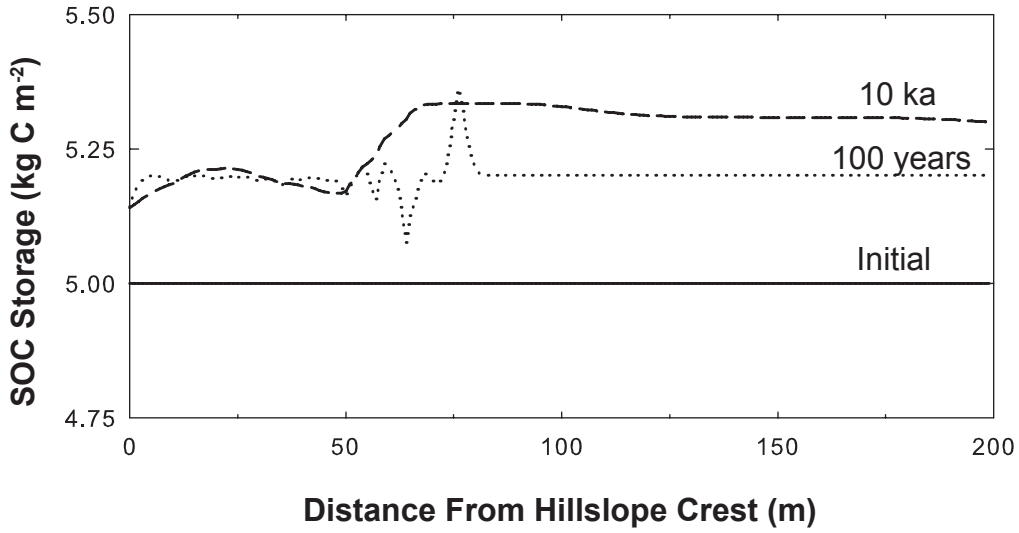

Figure 20. The effect of initial land surface roughness on organic carbon storage over short timescales. Perturbations in SOC storage caused from local land surface roughening are evident after 100 years but become smoothed by soil transport processes after 10 ka. The response of SOC storage to land surface roughening is thought to account for the variation in measured SOC storage values at LBL.

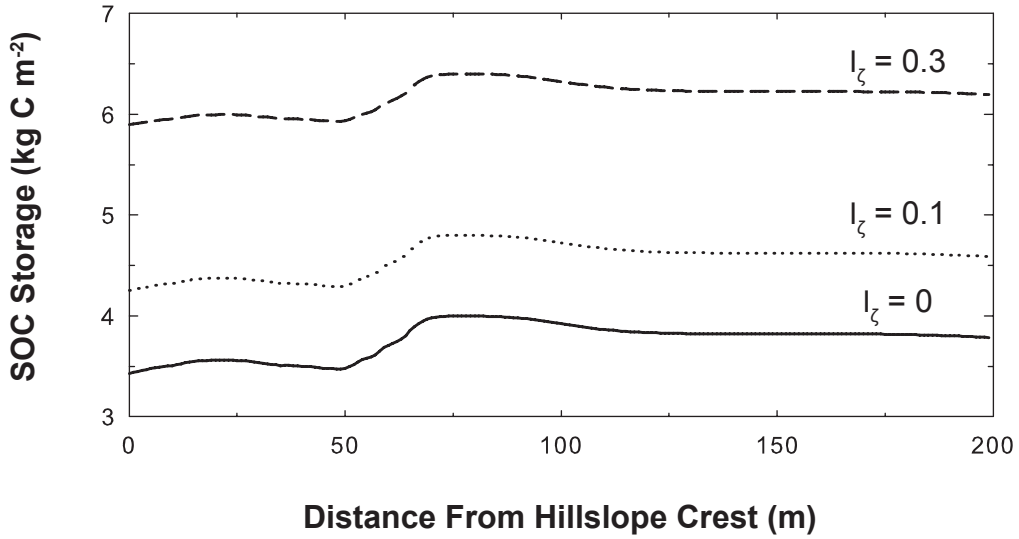

Figure 21. The effect of organic carbon flux across soil surface (I_ζ) on SOC storage after 10 ka. Changing the mass of carbon mixed into the soil at the surface shifts SOC storage without much alteration to variation in SOC storage with distance from hillslope crest.

Soil thickness has the potential to increase by 6-7 meters immediately adjacent to the initial hillslope toe. A maximum soil thickness on the order of 7 meters is reasonable given the change in elevation of the terrace close to the stream and the curvature inflection points for the Middle and Lower hillslopes (Figures 13 and14).

Soil Production

For thinning soils, the conversion of bedrock to soil essentially replaces the soil transported downslope. The higher the initial soil production rate (p_0), the faster eroded soil will be replaced. With an initial soil production rate of 50 m Ma^{-1}, soils on the convex up portion of the hillslope are significantly thinned (Figure 22). When initial soil production is an order of magnitude higher, soil thickness slowly increases at the hillslope crest (Figure 23). While soil organic carbon storage increases with distance from the hillslope crest for both initial soil production terms, the lower initial soil production term results in a greater difference in soil organic carbon storage between thinning and thickening soils.

In addition to a greater difference in soil organic carbon storage between thinning and thickening soils, the rate of change in soil organic carbon storage is much more abrupt with low initial soil production. As soils on the convex up portion of the hillslope slowly thicken, there is more soil to store organic carbon than when soils are thinned to, in some locations, one quarter the initial the soil thickness.

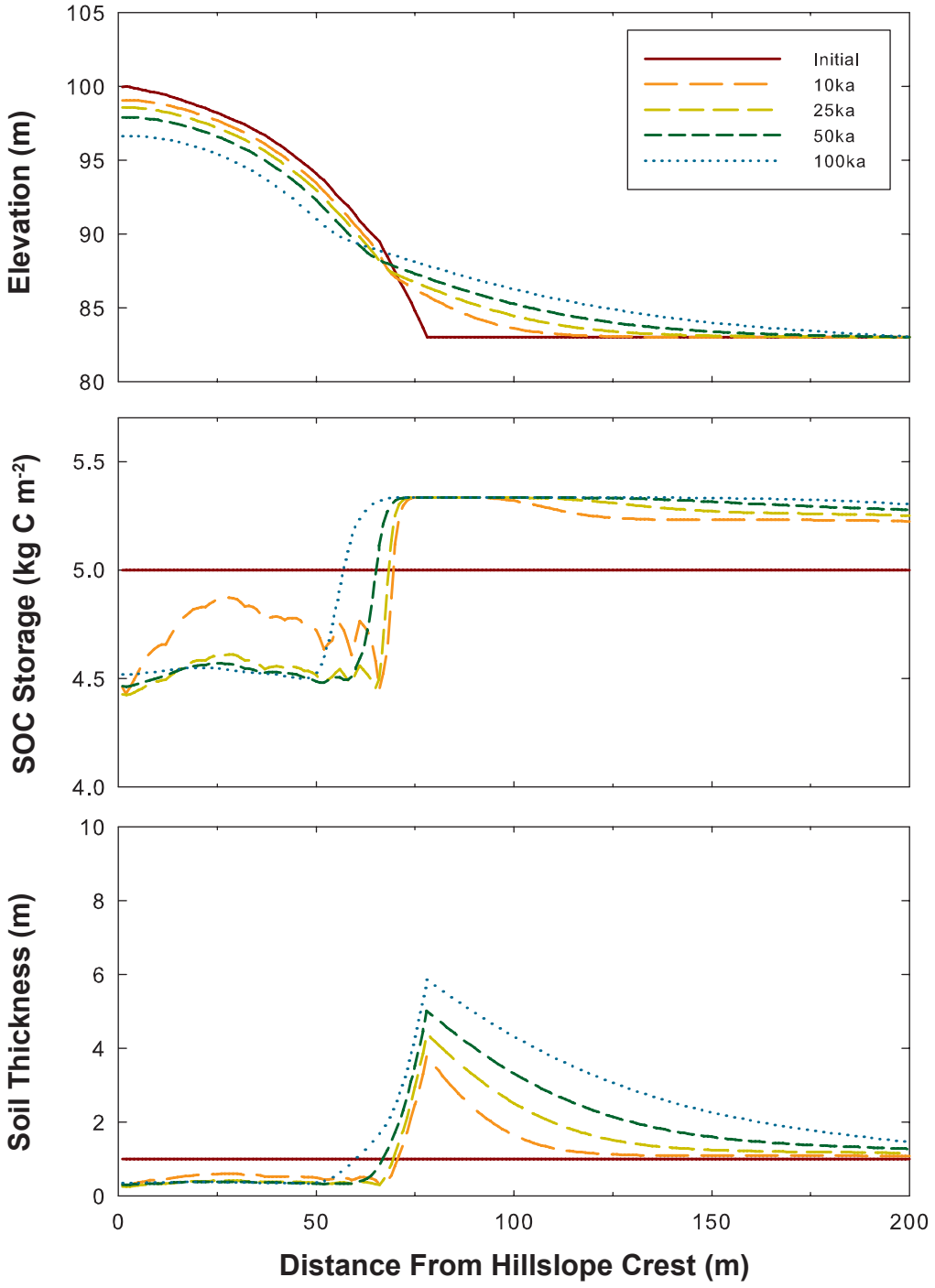

Figure 22. Plots of elevation (top), SOC storage (middle), and soil thickness (bottom) versus distance from hillslope crest showing the effect of SOC storage in thinned and thickened soils over 100 ka. (Parameters: $D = 0.01$; $p_0 = 50$ m Ma^{-1}; $\alpha = 0.3$; $\beta = 0.15$).

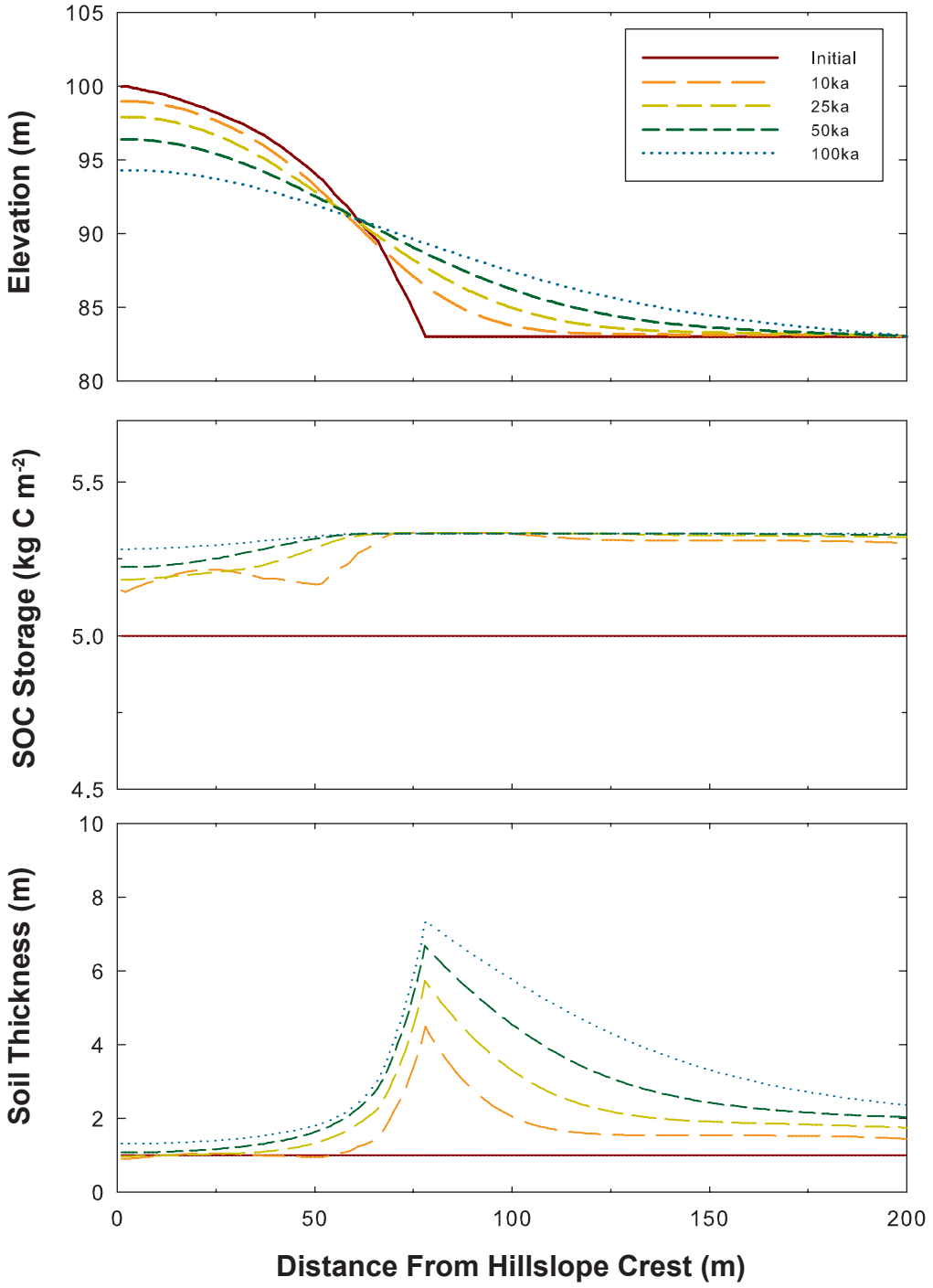

Figure 23. Plots of elevation (top), SOC storage (middle), and soil thickness (bottom) versus distance from hillslope crest showing the effect of initial soil production on SOC storages over 100 ka. Note that the difference in SOC storage between the convex and concave portions of the hillslope is less than in Figure 22. (Parameters: $D = 0.01$; $p_0 = 500$ m Ma^{-1}; $\alpha = 0.3$; $\beta = 0.15$).

e-*folding Depths of Organic Carbon Production and Respiration*

The *e*-folding depths of organic carbon production (α) and respiration (β) influence the storage of soil organic carbon. Holding all other parameters the same, soil organic carbon storage is lower with values of 0.5 m and 0.25 m for α and β, respectively (Figure 24) than with values of 0.3 and 0.15 for α and β (figure 23). Although the ratio between α and β is the same, β has a much stronger control on soil organic carbon storage than α. As the organic carbon produced within the soil increases with a higher α value, so does the respiration of organic carbon. This is due to organic carbon respiration being a function of the mass of organic carbon available for respiration. Coupling increasing carbon concentrations with increasing β results in a higher overall respiration relative to production despite the same ratio of α to β.

Diffusion Coefficient

Increasing the diffusion coefficient (*D*) speeds up hillslope evolution by increasing the rate of downslope soil transport. Increasing *D* by a factor of three requires that initial soil production must be kept high so that soils are not completely removed and the model remains stable. Despite having a high initial soil production rate (500 m Ma^{-1}), soils on the convex up portion of the hillslope thin during the first 25 ka when the diffusion coefficient is 0.03 (Figure 25). These soils thicken after 25 ka when the slope decreases as the hillslope evolves, resulting in less soil transported downslope from the convex up portion of the slope relative to the soil produced. Comparing this to a diffusion coefficient of 0.01 (Figure 24; all other variables the same), the lower diffusion coefficient results in immediate soil thickening over the entire hillslope. This initial

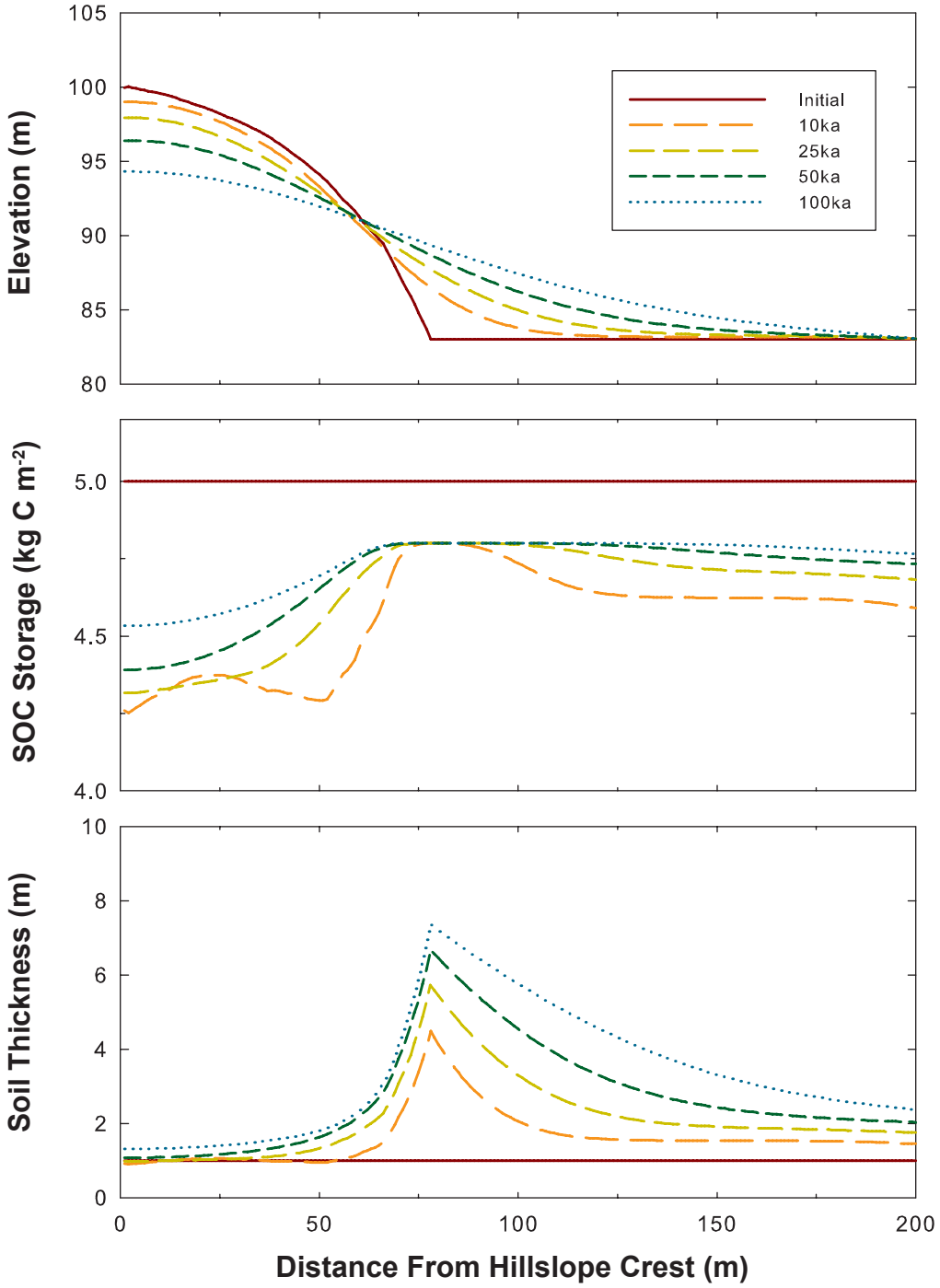

Figure 24. Plots of elevation (top), SOC storage (middle), and soil thickness (bottom) versus distance from hillslope crest showing the effect of α and β on SOC storages over 100 ka. Note that SOC storage values are lower than in Figure 23 with the same α :β ratio. (Parameters: $D = 0.01$; $p_0 = 500$ m Ma^{-1}; $\alpha = 0.5$; $\beta = 0.25$).

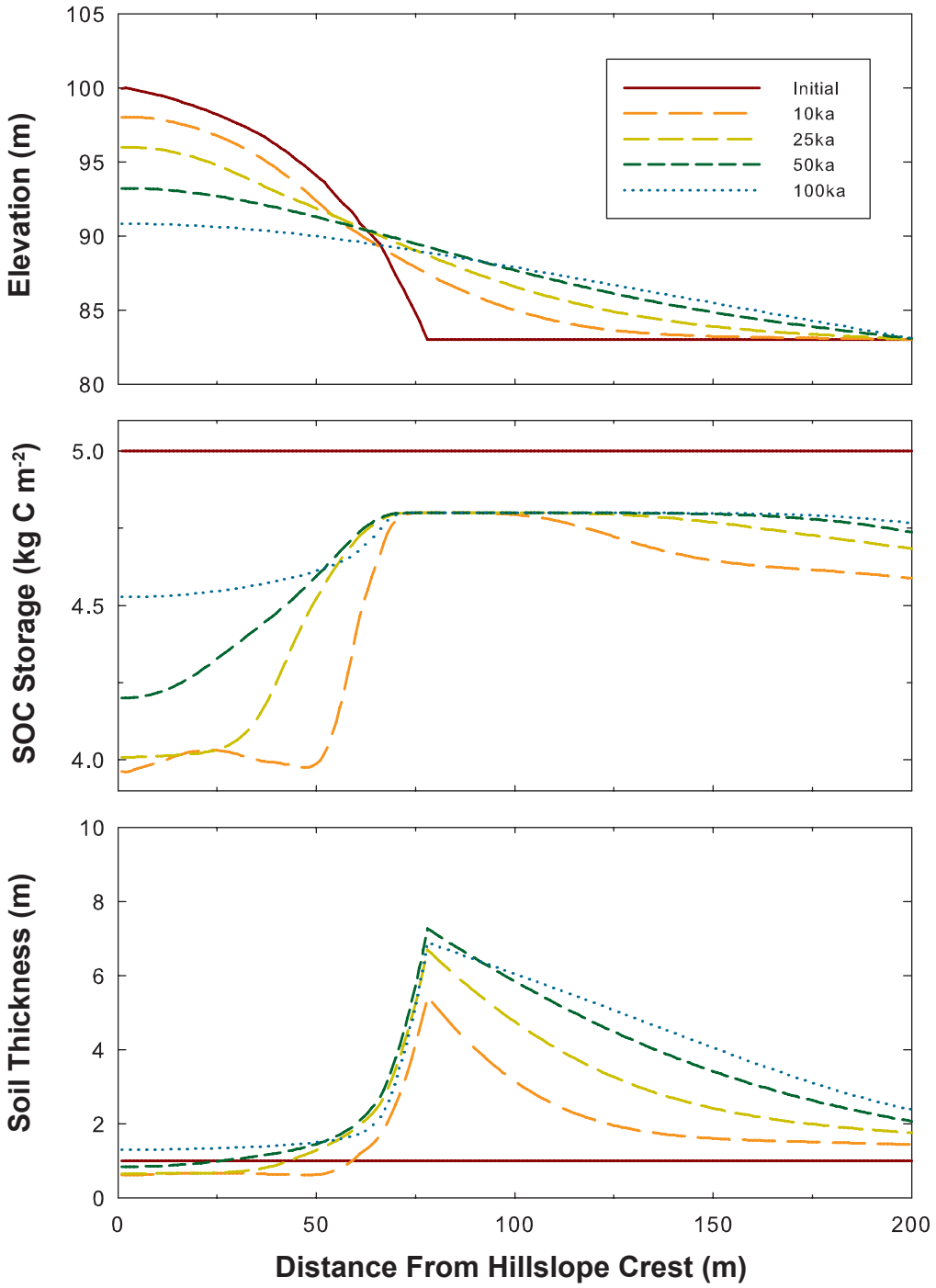

Figure 25. Plots of elevation (top), SOC storage (middle), and soil thickness (bottom) versus distance from hillslope crest showing the effect of increased diffusion coefficient on SOC storages over 100 ka. Increased rate of soil transport and hillslope evolution with increased D results in quicker upslope propagation of soil thickening environments than in Figure 24. (Parameters: $D = 0.03$; $p_0 = 500$ m Ma^{-1}; $\alpha = 0.5$; $\beta = 0.25$).

thinning with an increased diffusion coefficient results in less soil organic carbon storage on the convex portion of the hillslope (Figure 25). The higher rates of soil transport, however, result in soil organic carbon storage increasing at a quicker rate on the convex portion of the slope. After 100 ka has elapsed, both simulations have approximately the same total soil organic carbon storage. The soil thickness peak at the toe of the hillslope is broader with a higher diffusion coefficient. This broader soil thickness peak is reflected in higher soil organic carbon storage downslope of the peak compared to storage involving a lower diffusion coefficient after the same duration of time.

The occurrence of worms in soil pits was observed only in the lower elevation pits of the Middle and Lower hillslopes. This is attributed to higher soil moisture toward the hillslope toe and implies that the mixing activity of worms, and thus the diffusion coefficient, may increase downslope. Simulating a linear increase in the diffusion coefficient from 0.01 at the hillslope crest to 0.03 at 100 m from the crest (then held constant at 0.03 for the remaining distance), creates a significant difference in soil organic carbon storage between thinning and thickening soil (Figure 26). Soil production for this simulation was 50 m Ma^{-1}. Increasing diffusivity with distance without making soil production high, results in a difference of 1 kg C m^{-2} in soil organic carbon storage between thinning and thickening soils, the highest difference of all the simulations discussed. Increasing diffusivity with distance also results in a peak in soil organic carbon storage after 10 ka that becomes smoothed as time progresses to 100 ka. The amount of organic carbon stored on the terrace surface downslope of the soil thickness peak increases over the same timescale. In most other simulations, this portion of the hillslope quickly nears equilibrium between organic carbon inputs and outputs, such that there is

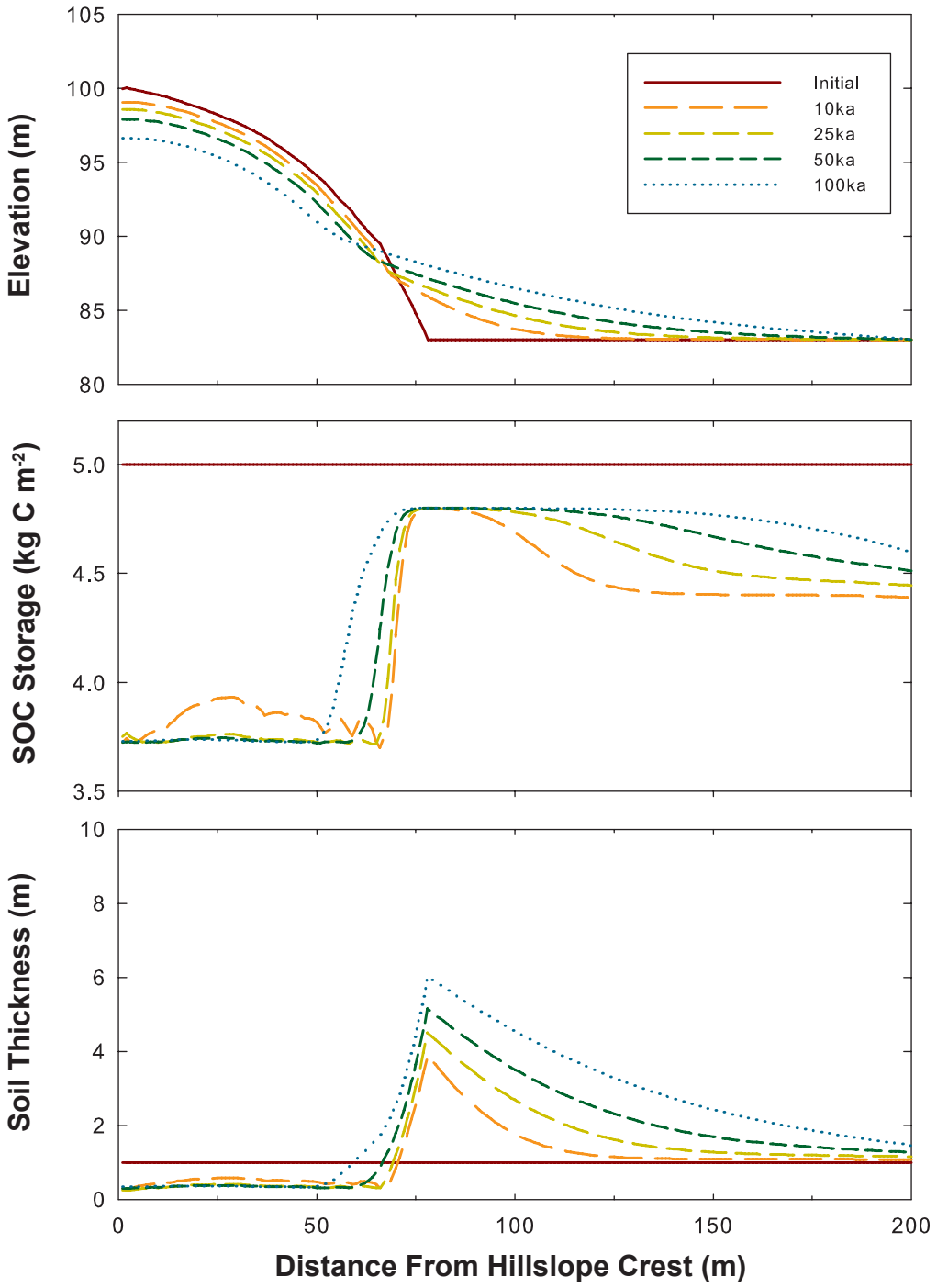

Figure 26. Plots of elevation (top), SOC storage (middle), and soil thickness (bottom) versus distance from hillslope crest showing the effect of linearly increasing the diffusion coefficient with distance on SOC storages over 100 ka. *D* was increased from 0.01 to 0.03 over the distance 0-100 m then held constant at 0.03 over the distance 100-200 m. SOC storage increases 1 kg C m^{-2} between locations of soil thinning and soil thickening (Parameters: D = 0.01-0.03; p_0 = 50 m Ma^{-1}; α = 0.5; β = 0.25).

not a significant increase in soil organic carbon storage on the terrace surface after 10 ka. The downslope migration of the location of soil thickening means that the soil organic carbon storage increases more over time on what was the terrace surface than in the location of soil thickening that propagates upslope, as seen in Figure 22 and Figure 23.

Incision

Soil organic carbon storage decreases with distance from the hillslope crest and with increasing time when a hillslope is responding to active incision (Figure 27). As a flat surface was incised at a rate of 30 m Ma^{-1}, soil thickness and soil organic carbon storage immediately decreased at the site of incision. The conversion of bedrock to soil resulted in soil lofting and thickening where the land surface remained flat. Soil organic carbon storage increased in thickening soils until soil transport propagated to the hillslope crest and the entire hillslope began lowering between 100 and 500 ka Soil organic carbon storage for the entire hillslope decreased once the hillslope crest began lowering. After 1 Ma, soil organic carbon storage over the entire hillslope is approximately constant at ~3.75 kg C m^{-2}. It should be noted that although soil thickness does not increase, there is a slight increase in soil organic carbon storage in the last 10 m of the hillslope adjacent to the stream. This is likely caused by increased slope and soil transport adjacent to the stream.

Comparison of Modeled and Measured Soil Organic Carbon Storage

Modeled soil organic carbon storage is 5-30% greater in locations of soil thickening than soil organic carbon storage where thinning occurs. After the perturbations

in initial land surface roughness dissipate, soil organic carbon storage remains smooth in model simulations. In a natural setting, surface roughness and the associated organic carbon perturbations would be expected to show up continually through time across the entire hillslope. The large amount of variability seen in calculated soil organic carbon storage for the study area (Figure 18) is likely a result of local surface roughness. In the same way that bulk density measurements represent a 'snapshot' of soil lofting and settling processes, calculated SOC storage values represent a 'snapshot' of the response of organic carbon storage to surface roughening processes, e.g. tree throw, and soil smoothing processes, e.g. soil transport.

Calculated soil organic carbon storage values show an overall increasing trend with distance from the hillslope crest and curvature, similar to model results (Figures 18 and 28). A linear regression of all soil pits suggests an increase in organic carbon storage on the order of 10% (Figure 18), within the range of model predictions. Measured organic carbon storage agrees with model results, than locations of soil thickening have greater potential to sequester organic carbon that thinning environments.

In all model simulations, organic carbon storage reaches a maximum value for the concave portions of the slope all the way to the end of the terrace surface. This suggests that the control of physical transport on storing organic carbon in soil over geomorphic timescales is not so much in the transport of carbon-rich soil, but rather in the creation of thicker soils capable of accommodating more organic carbon. Furthermore, despite continued thickening, organic carbon storage remains constant once a maximum value is reached. This is consistent with the idea that organic carbon respiration occurs at a significantly shorter timescale than soil transport.

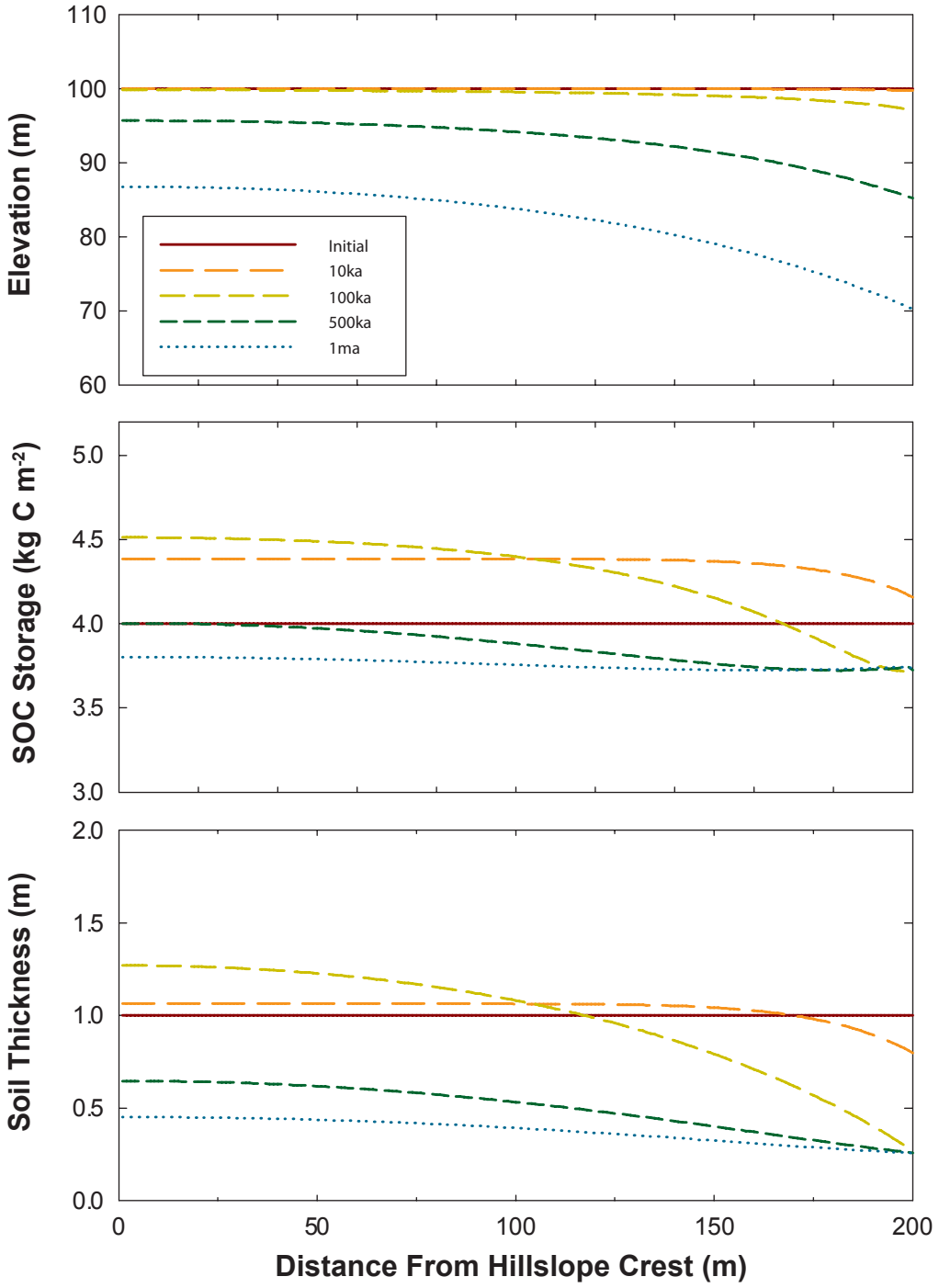

Figure 27. Plots of elevation (top), SOC storage (middle), and soil thickness (bottom) versus distance from hillslope crest showing the effect of incision on SOC storages over 1 Ma. (Parameters: D = 0.01-0.03; p_0 = 50 m Ma^{-1}; α = 0.5; β = 0.25; Incision (I) = 30 m Ma^{-1}).

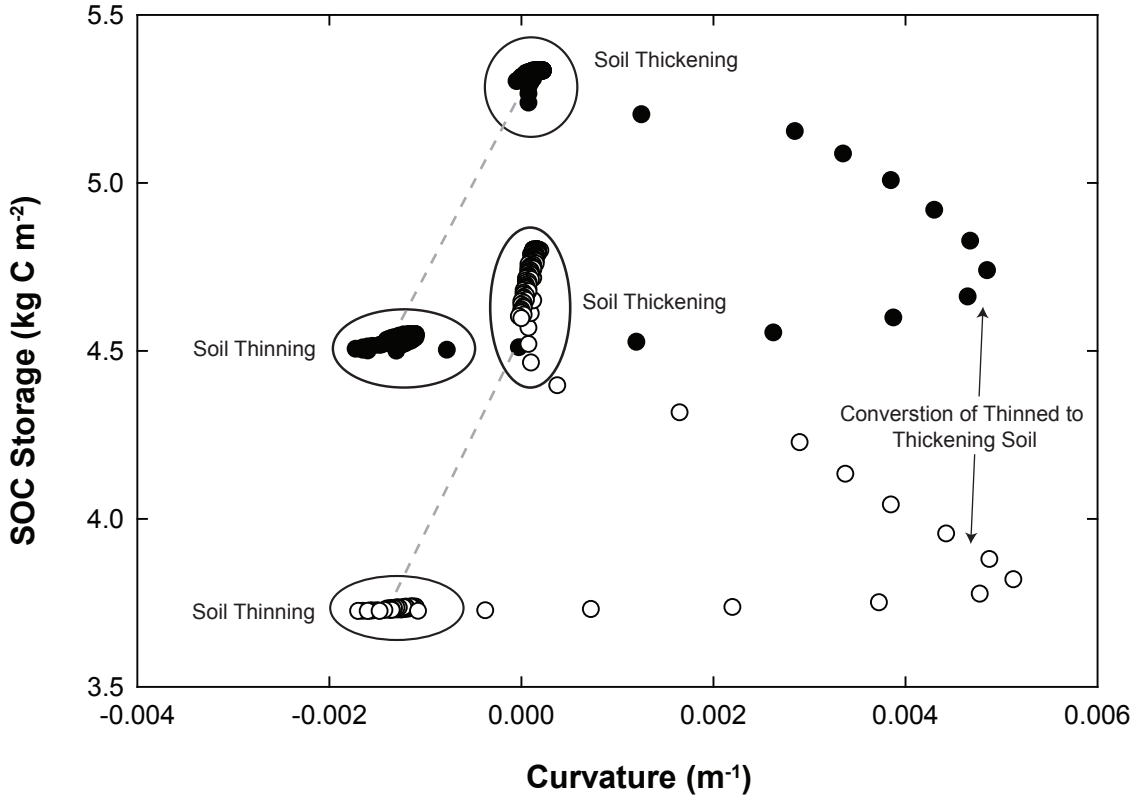

Figure 28. Plot of curvature versus SOC Storage for model simulations presented in Figure 22 (closed circle) and Figure 26 (open circle) after 100 ka. Recall that both simulations have an initial soil production of 50 m Ma^{-1} and experienced locations of thinning and thickening soils. The dashed line represents the increase in SOC storage after a thinned soil on the convex portion of the hillslope is converted to a location of soil thickening at the concave toe and on the terrace surface.

The Role of Physical Processes on Soil Carbon Cycling

Although most of the physical processes responsible for soil mixing and transport are biomechanical, these processes appear to exert a stronger control on the amount of organic carbon stored in soils than the biological production and decomposition processes. The balance between *e*-folding depths of carbon production and respiration determines the amount of carbon a soil can potentially store. In turn, the *e*-folding depth can be viewed as being controlled by soil mixing processes and physical soil properties. Additionally, the flux of organic carbon across the soil surface interface is a purely mechanical processes independent of carbon production, assuming there is litter on the soil surface.

It is important to consider the fluvial relationship with hillslopes when considering organic carbon storage on a hillslope through time. Not only does the fluvial environment posses the potential to accommodate soil organic carbon storage with the creation of terrace and flood plain surfaces but it also can contribute to releasing stored organic carbon when the stream migrates into terraces and hillslope toes. The periodic removal of thickened soil and organic carbon from the depositional hollows of Yoo et al. (2005, 2005) occurs on the order of every 10 ka. While landsliding is absent at LBL, the cross-valley migration of the stream results in the periodic removal of thickened soil at the study area. While time constraints on fluvial migration of Panther Creek are absent, it is important to note that even if periodic removal occurred on the order of 10 ka, modeling shows that the organic carbon storage of the hillslope toe is usually close to a maximum within that time frame. Furthermore, the oversteepening of hillslopes by active stream undercutting would result in accelerated soil transport during the early stages of

hillslope relaxation onto the terrace surface. If this accelerated soil transport results in soil thickening on a timescale shorter than that of organic carbon cycling, the first few thousand years of hillslope evolution after terrace formation may involve significant organic carbon sequestration. More work is needed on the complex fluvial environment of LBL to understand the details of this relationship.

CHAPTER V

CONCLUSIONS

The primary objective of this study was to derive a mass-balance model describing the downslope transport of soil organic carbon coupled with biogenic carbon production and respiration. The elements of this mass-balance model include the transport of organic carbon in or out of a control volume, the flux of organic carbon across the soil surface, production of organic carbon within the soil, and respiration of organic carbon within the soil. Numerical model simulations illustrate these elements involved in organic carbon conservation collectively influence the cycling of carbon in hillslope soils.

Comparisons of field data to model results suggest that locations of soil thickening store more organic carbon than locations of soil thinning. It is in the conversion of thinned soils to sites of soil thickening where the potential is created to significantly increase soil organic carbon storage through time. This occurred in most model simulations by the upslope propogation of the location of soil thickening, which is strongly controlled by soil transport. The variability in measured soil organic carbon storage represents a ‘snapshot’ of processes creating local soil carbon variability and processes that smooth this variability. Modeling shows that variability in soil organic carbon storage arises in less than 100 years, a result of soil transport responding to initial land surface roughness created by soil mixing processes, e.g. tree throw and burrowing. As this initial land surface roughness is smoothed through time by soil transport in model simulations, so is the variability in soil organic carbon storage.

Although many of the model components are a function of biological processes, it is the biomechanical soil mixing processes that are important in soil organic carbon storage in forested hillslope soil. The difference in characteristic timescales of soil mixing and biologic carbon production/respiration processes causes soil transport to have greater control on the amount of organic carbon stored in soil. The flux of organic carbon across the soil surface is limited by soil mixing rates at the soil-surface interface, not by the amount of biomass present on the soil surface. The *e*-folding depths of organic carbon production and respiration are related to the depth to which biomechanical soil mixing processes move organic carbon downward before carbon is decomposed.

This study shows that physical soil transport processes also influence soil organic carbon storage at different timescales. For example, soil transport on the timescale of biomechanical soil mixing influences the maximum organic carbon storage of soils, whereas soil transport on the hillslope evolution timescale influences the organic carbon storage of soils through time. Soil transport therefore has the potential to influence soil organic carbon storage over human and geologic timescales. Over the evolution of a hillslope, soil organic carbon storage potentially increases by 5-25% in thinned soils converted to locations of soil thickening. This increase may be higher on hillslopes reclaimed from agriculture or deforestation and suggests that forested hillslopes may sequester significant atmospheric carbon dioxide.

APPENDIX A.

SUMMARY OF SOIL PIT DATA

Table A1-1. Summary of field data for the Upper, Middle, and Lower hillslopes.

Sample	Average Sampling Depth (cm)	Depth Interval	Bulk Density (g cm-3)	Mass Fraction >2mm	% Organic Carbon	%Nitrogen	C:N Molar Ratio	SOC Storage for Intervals (kgC m-2)	Distance from Hillslope Crest (m)	Curvature (m-1)
Upper Hillslope										
08JR08									22	-0.00252
A	2.875	0-5cm	0.815		2.67	0.27	11.65	1.088		
B	7.5	5-15cm	1.075		0.54	0.25	2.47	0.488		
C	12.5	5-15cm	0.981		0.41	0.09	5.13			
D	17.5	15-30cm	1.187		0.26	0.13	2.30			
E	22.5	15-30cm	1.027		0.51	0.21	2.82	0.594		
F	27.5	15-30cm	1.056		0.32	0.11	3.32			
G	32.5	30-50cm	0.967		0.46	0.15	3.51	0.651		
H	42.5	30-50cm	0.841		0.26	0.13	2.43			
I	52.5	50-80cm	1.253		0.22	0.14	1.84	0.827		
08JR09									37	-0.00432
A	2.9	0-5cm	0.732		3.87	0.23	19.89	1.417		
B	7.5	5-15cm	1.066		1.08	0.24	5.34	0.898		
C	12.5	5-15cm	1.252		0.47	0.26	2.08			
D	17.5	15-30cm	1.085		0.91	0.15	7.24			
E	22.5	15-30cm	1.128		0.58	0.18	3.74	0.994		
F	27.5	15-30cm	0.968	0.229	0.54	0.24	2.69			
G	32.5	30-50cm	1.193		0.32	0.22	1.72			
H	37.5	30-50cm	1.200		0.31	0.16	2.23	0.769		
I	42.5	30-50cm	1.140		0.35	0.19	2.19			
08JR10									55	-0.02536
A	2.9	0-5cm	0.771		2.08	0.25	9.67	0.802		
B	7.5	5-15cm	0.794		0.62	0.19	3.82	0.586		
C	12.5	5-15cm	1.159		0.58	0.22	3.06			
D	17.5	15-30cm	1.075*	0.300*	0.36	0.45	0.94			
E	22.5	15-30cm	1.075*	0.300*	0.25	0.24	1.22	0.320		
F	27.5	15-30cm	1.075*	0.300*	0.24	0.32	0.87			
G	32.5	30-50cm	1.068*	0.300*	0.23	0.15	1.84			
H	37.5	30-50cm	1.068*	0.300*	0.3	0.22	1.58	0.379		
I	42.5	30-50cm	1.068*	0.300*	0.23	0.2	1.35			
J	47.5	50-80cm	1.25*	0.300*	0.39	0.17	2.72	0.171		

* Denotes averaged values used in SOC storage calculations

Table A1-1 continued.

Sample	Average Sampling Depth (cm)	Depth Interval	Bulk Density (g cm-3)	Mass Fraction >2mm	% Organic Carbon	%Nitrogen	C:N Molar Ratio	SOC Storage for Intervals (kgC m-2)	Distance from Hillslope Crest (m)	Curvature (m-1)
08JR11									73	-0.01490
A	2.875	0-5cm	0.854	0.141	3.25	0.3	12.75	1.192		
B	7.5	5-15cm	1.129	0.159	2.01	0.25	9.25	1.401		
C	12.5	5-15cm	1.261	0.218	0.88	0.23	4.48			
D	20	15-30cm	1075*	0.300*	0.51	0.23	2.60	0.485		
E	25	15-30cm	1075*	0.300*	0.49	0.2	2.88			
F	30	15-30cm	1075*	0.300*	0.29	0.26	1.31			
G	35	30-50cm	1068*	0.300*	0.29	0.19	1.80	0.303		
H	40	30-50cm	1068*	0.300*	0.23	0.15	1.82			
I	45	30-50cm	1068*	0.300*	0.17	0.12	1.61			
J	50	30-50cm	1068*	0.300*	0.12	0.17	0.85			
Middle Hillslope										
08JR01									3	0.00447
A	2.9	0-5cm	0.742	0.885	4.21	0.25	19.95	1.357		
B	7.5	5-15cm	0.990	1.111	0.92	0.17	6.19	0.728		
C	12.5	5-15cm	1.112	1.189	0.62	0.06	11.60			
D	17.5	15-30	0.986	1.146	0.35	0.08	5.15	0.439		
E	36.5	30-50cm	1.142	1.191	0.08	0.16	0.61	0.169		
08JR02									14	-0.00716
A	2.9	0-5cm	0.789	0.264	3.99	0.22	20.79	1.158		
B	7.5	5-15cm	1.042	0.083	0.96	0.11	10.13	0.662		
C	12.5	5-15cm	0.879	0.161	0.61	0.19	3.85			
D	17.5	15-30cm	1.048	0.224	0.7	0.16	5.05	0.758		
E	22.5	15-30cm	1.127	0.085	0.4	0.14	3.35			
F	30.5	30-50cm	1.338	0.199	0.64	0.09	8.96	1.371		

* Denotes averaged values used in SOC storage calculations

Table A1-1 continued.

Sample	Average Sampling Depth (cm)	Depth Interval	Bulk Density (g cm-3)	Mass Fraction >2mm	% Organic Carbon	%Nitrogen	C:N Molar Ratio	SOC Storage for Intervals (kgC m-2)	Distance from Hillslope Crest (m)	Curvature (m-1)
08JR03									25	-0.00836
	2.9*	0-5cm*	0.779*	0.192*				1.043		
B	7.5	5-15cm	1.163	0.282	1.05	0.11	11.45	0.546		
C	12.5	5-15cm	0.969	0.477	0.6	0.08	8.37			
D	20.0	15-30cm	1.189*	0.343*	0.39	0.1	4.45	0.311		
E	30.0	15-30cm	1.189*	0.343*	0.14	0.05	3.57			
F	40.5	30-50cm	1.172	0.245	1.03	0.17	7.23	0.816		
G	47.5	30-50cm	1.045	0.366	0.03	0.15	0.23			
08JR04									48	0.00479
A	2.9	0-5cm	1.001	0.292	3.22	0.26	14.39	1.141		
B	9.5	5-15cm	1.134	0.165	1.52	0.16	11.06	1.439		
C	18.5	15-30cm	1.137	0.217	0.79	0.11	8.64	1.056		
D	37.5	30-50cm	0.971	0.198	0.34	0.15	2.60	0.530		
08JR05									63	0.00579
A	2.9	0-5cm	0.706	0.196	3.36	0.29	13.66	0.953		
B	7.5	5-15cm	0.951	0.048	1.15	0.21	6.33	0.886		
C	12.5	5-15cm	1.220	0.098	0.61	0.2	3.55			
D	17.5	15-30cm	1.356	0.079	0.34	0.1	4.08			
E	22.5	15-30cm	1.297	0.057	0.23	0.15	1.82	0.594		
F	27.5	15-30cm	1.261	0.105	0.42	0.19	2.56			
G	32.5	30-50cm	1.283	0.046	1.38	0.17	9.54	1.965		
H	42.5	30-50cm	1.396	0.049	0.16	0.11	1.63			
I	52.5	50-80cm	1.362	0.048	0.16	0.07	2.87	0.319		
J	62.5	50-80cm	1.466	0.073	0					
08JR06									75	0.00711
A	2.9	0-5cm	0.906	0.010	3.23	0.28	13.36	1.449		
B	7.5	5-15cm	0.897	0.011	1.23	0.14	10.34	1.165		
C	12.5	5-15cm	1.135	0.003	1.08	0.26	4.89			
D	17.5	15-30cm	1.139	0.011	0.67	0.44	1.81	1.132		
E	32.5	30-50cm	1.180	0.002	0.2			0.499		
F	42.5	30-50cm	1.260	0.003	0.21					

* Denotes averaged values used in SOC storage calculations

Table A1-1 continued.

Sample	Average Sampling Depth (cm)	Depth Interval	Bulk Density (g cm-3)	Mass Fraction >2mm	% Organic Carbon	%Nitrogen	C:N Molar Ratio	SOC Storage for Intervals (kgC m-2)	Distance from Hillslope Crest (m)	Curvature (m-1)
08JR06 continued										
G	52.5	50-80cm	1.312	0.003	0.54					
H	62.5	50-80cm	1.480	0.008	0.61			1.103		
I	67.5	50-80cm	1.328	0.013	0.47					
Lower Hillslope										
08JR012									4	-0.01054
A	2.9	0-5cm	0.709	0.042	3.53	0.04	25.22	1.198		
B	7.5	5-15cm	1.037	0.018	1.4			1.295		
C	12.5	5-15cm	1.187	0	0.95					
D	17.5	15-30cm	0.854	0	0.89					
E	22.5	15-30cm	0.790	0	0.49			0.803		
F	27.5	15-30cm	0.864	0	0.54	0.04	16.03			
G	32.5	30-50cm	1.195	0	0.73					
H	37.5	30-50cm	0.999	0	0.51			1.341		
I	45.0	30-50cm	1.120*	0*	0.56	0.1	6.92			
J	50.0	30-50cm	1.120*	0*	0.62					
08JR013									23	-0.00357
A	2.9	0-5cm	0.525	0.056	2.18			0.541		
B	7.5	5-15cm	0.572	0.037	1.7			1.089		
C	12.5	5-15cm	1.205	0	0.81					
D	17.5	15-30cm	1.089	0	0.57					
E	22.5	15-30cm	1.109	0	0.5			0.893		
F	27.5	15-30cm	0.982	0	0.62					
D	17.5	15-30cm	1.089	0	0.57					
E	22.5	15-30cm	1.109	0	0.5			0.893		
F	27.5	15-30cm	0.982	0	0.62					

* Denotes averaged values used in SOC storage calculations

Table A1-1 continued.

Sample	Average Sampling Depth (cm)	Depth Interval	Bulk Density (g cm-3)	Mass Fraction >2mm	% Organic Carbon	%Nitrogen	C:N Molar Ratio	SOC Storage for Intervals (kgC m-2)	Distance from Hillslope Crest (m)	Curvature (m-1)
08JR014									47	0
A	2.85	0-5cm	0.835	0.046	3.92			1.561		
B	7.5	5-15cm	0.572	0.052	1.51			1.007		
C	12.5	5-15cm	1.063	0	1.04					
D	17.5	15-30cm	1.113	0.013	1.22			1.370		
E	25	15-30cm	1.012*	0*	0.51					
F	32.5	30-50cm	1.272	0.024	0.35			0.711		
G	42.5	30-50cm	1.012*	0*	0.28					
08JR015									70	0.01122
A	2.85	0-5cm	0.568	0.236	2.66			0.577		
B	7.5	5-15cm	0.991	0.071	1.44			1.271		
C	12.5	5-15cm	1.263	0.110	1.04					
D	17.5	15-30cm	1.057	0.059	0.56			0.569		
E	25	15-30cm	1.012*	0*	0.34					
F	30	15-30cm	1.012*	0	0.23					
G	35	30-50cm	1.120*	0*	0.28			0.616		
H	40	30-50cm	1.120*	0*	0.27					
09JR01									86.5	0.00709
A	2.9	0-5cm	0.816	0.063	4.8			1.835		
B	7.5	5-15cm	1.146	0.017	1.23			1.221		
C	12.5	5-15cm	1.085	0.011	0.99					
E	27.5	15-30cm	1.248	0	0.45			0.843		
F	37.5	30-50cm	1.232	0	0.81			0.958		
K	45	30-50cm	1.181	0	0.19					
G	50	30-50cm	1.120*	0*	0.22					
H	60	50-80cm	1.367*	0*	0.48			1.039		
I	70	50-80cm	1.367*	0*	0.1					
J	80	50-80cm	1.367*	0*	0.18					
Organic Matter										
09JR01-A	0cm				40.21	1.71	27.48			
Roots										
08JR12-B	7.5				46.94	0.81	24.62			

* Denotes averaged values used in SOC storage calculations

APPENDIX B

MATLAB CODE

```
% Organic carbon in hillslope soil
% Written by John Roseberry, David Furbish

%Relaxation of a hillslope onto a fluvial terrace

D0 = 0.01;                          % initial diffusion coefficient
theta = 0;                          %   rate of change of D with distance from hillslope
Po = 0.00005;                       %  initial soil production rate (m/yr)
Gamma0 =0.5;                        %  e-folding depth of soil production
c_eta = 0.7;                        %  volumetric concentration of soil particles at eta
c_bar = 0.5;                        %  depth-averaged volumetric concentration of soil
                                    particles
I =  0 ;                            %  stream incision rate (m/yr)
Z_initial =   83;                   %  Initial elevation (m) of stream
Z_final =   83;                     %  Final elevation (m) of stream when incision ends
n_stream =   79 ;                   %  Node where stream begins
OC_eta = 0;                         %  Mass fraction of Organic Carbon at eta
I0 = 1;                             %  Initial organic carbon input rate by production
                                    in soil (kg C m-2 yr-1)
alpha = 0.5;                        %  e-folding depth of OC input by production in
                                    soil (m)
R0 = 1;                             %  Initial organic carbon respiration rate (yr-1)
beta = 0.25;                        %  e-folding depth of OC respiration (m)
I_zeta0 = 0.1;                      %  initial flux of carbon across surface at left node
                                    (kg/yr)
depth_transport = 1 ;               %The depth to the base of the active layer (m)

dx = 1;                             %  space interval in meters
dt = 1;                             %  time interval in years
N = 202;                            %   number of nodes
Nt = 100000;                %  Number of time steps

%  Change D with position on hillslope
for i=1:100
   D(i) = D0 + theta*x(i);
end
for i=101:N
   D(i) = D(i-1);
end
```

```
%Boundary conditions for surface elevation
zold(2) = 100; %left boundary condition for surface elevation
zold(202) = Z_initial; %Right boundary condition for surface elevation

%Initial condition for land surface elevation from the Upper hillslope transect
for i=3:12
   zold(i) =zold(i-1)-0.058;
end
for i=13:22
   zold(i) = zold(i-1) - 0.0905;
end
for i=23:27
   zold(i) = zold(i-1) - 0.109;
end
for i=28:32
   zold(i) = zold(i-1) - 0.115;
end
for i=33:37
   zold(i) = zold (i-1) - 0.14;
end
for i=38:42
   zold(i) = zold(i-1) - 0.183;
end
for i=43:47
   zold(i) = zold(i-1) - 0.203;
end
for i=48:52
   zold(i) = zold(i-1) - 0.227;
end
for i=53:54
   zold(i) = zold(i-1) - 0.303;
end
for i=55:56
   zold(i) = zold(i-1) - 0.3125;
end

for i=57:59
   zold(i) = zold(i-1) - 0.253;
end
for i=60:61
   zold(i) = zold(i-1) - 0.38;
end
for i=62:66
   zold(i) = zold(i-1) - 0.282;
```

```
end
for i=67:68
   zold(i) = zold(i-1) - 0.5;
end
for i=69:70
   zold(i) = zold(i-1) - 0.548;
end
for i=71:73
   zold(i) = zold(i-1) - 0.50;
end
for i=74:76
   zold(i) = zold(i-1) - 0.54;
end
for i=76:78
   zold(i) = zold(i-1) - 0.57;
end
for i=n_stream:201
   zold(i) = Z_initial;
end


%Initial conditions for soil thickness, hold
for i=1:N;
   hold(i)=1;
end

%Initial condition for mechanically active soil thickness, h_aold
for i=1:N;
  h_aold(i) = 1;
end

 %initial condition for eta, eold
for i=1:N
   eold(i) = zold(i) - hold(i);
end

%initial condition for Organic Carbon Storage
for i=1:N;
   OCold(i) = 5;
end


V = 0; %Initialize video counter

flag = 0;
```

```
for k=1:Nt

  % Set conditions for stream incision
  if flag == 0
      if I >0
      for i=n_stream:202
          zold(i) = Z_initial - I*k*dt;
          if zold(i) <= Z_final
              zold(i) = Z_final;
              flag = 1;
          end
      end
      end
   end


    %Solve for land surface elevation (znew) and calculate new eta (enew) and soil
thickeness (hnew).
    for i=2:N-1; %Step through space
      znew(i) = zold(i)+(dt*D(i)/(2*c_bar*dx^2))*((h_aold(i)+h_aold(i+1))*(zold(i+1)...
        -zold(i))-(h_aold(i)+h_aold(i-1))*(zold(i)-zold(i-1)))...
        -dt*((c_eta/c_bar)-1)*(-Po*exp(-hold(i)/Gamma(i)));
      enew(i) = eold(i) - dt*Po*exp(-hold(i)/Gamma(i));
      hnew(i) = zold(i) - eold(i);

     % Conditions for soil thickness value used in next time step
      if hnew(i) >= depth_transport
          h_anew(i) = depth_transport;
      else h_anew(i) = hnew(i);
      end

    end

    % Solve for new organic carbon storage (OCnew)
    for i=2:N-1;
       OCnew(i) = OCold(i) + (dt*D(i)/(2*c_bar*dx^2))*...
       ((OCold(i)+OCold(i+1))*(h_aold(i)/hold(i))*(zold(i+1)-zold(i))...
       -(OCold(i)+OCold(i-1))*(h_aold(i)/hold(i))*(zold(i)-zold(i-1)))...
       + ((dt*c_eta*OC_eta/c_bar)*(-Po*exp(-hold(i)/Gamma(i))))...
       + I_zeta(i)*dt/c_bar + (dt*I0*alpha/c_bar)*(1-exp(-hold(i)/alpha))...
       - (dt*R0*beta*OCold(i))*(1-exp(-hold(i)/beta));
    end
```

```
% Replace old values with new values
   znew(1) = znew(3);
   enew(1) = enew(3);
   hnew(1) = hnew(3);
   h_anew(1) = h_anew(3);
   OCnew(1) = OCnew(3);

  enew(202) = eold(202) - dt*Po*exp(-hold(202)/Gamma(202));
   hnew(202) = zold(202) - enew(202);
   OCnew(202) = OCold(202);

      if hnew(202) >= depth_transport(202)
          h_anew(202) = depth_transport(202);
       else h_anew(202) = hnew(202);
       end

   for i=1:N-1;
       zold(i) = znew(i);
       hold(i) = hnew(i);
       eold(i) = enew(i);
       h_aold(i) = h_anew(i);
       OCold(i) = OCnew(i);
   end

   hold(1) = hnew(1);
   hold(202) = hnew(202);
   eold(202) = enew(202);
   h_aold(202) = h_anew(202);
   OCold(1) = OCnew(1);
   OCold(202) = OCnew(202);

% Create movie plotting changes in organic carbon storage and soil thickness
   tempV = mod(k,100);
   if tempV == 0
       V = V + 1;
       plot(x,OCold,x,hold);
      axis([0,200,0,8]);
       Mov(V) = getframe;
   end
end
```

APPENDIX B

FIELD SITE LOCATIONS

The field area is located on the north side of US-79 west of Dover, TN. A locked service road operated by Land Between the Lakes National Recreation Area is a suitable place to pull off of US-79 and enter the park on foot. This pullout is located 11.7 km west of the intersection of US-79 and TN-49 (Spring Street) in downtown Dover, TN (6.8 km west of where The Trace/TN-49 heads north to the LBL visitor center) or 8.1 km east from the end of the US-79 bridge crossing Kentucky Lake/Tennessee River. The service road is situated between two intersections of US-79 with Old State Route 76.

GPS Locations in coordinate system WGS 1984 UTM Zone 16N:

Upper Hillslope
Northing 4037616
Easting 41337
Bearing of Transect: 335°

Middle Hillslope
Northing 4038168
Easting 413327
Bearing of Transect: 058°

Lower Hillslope
Northing 4038338
Easting 413251
Bearing of Transect: 040°

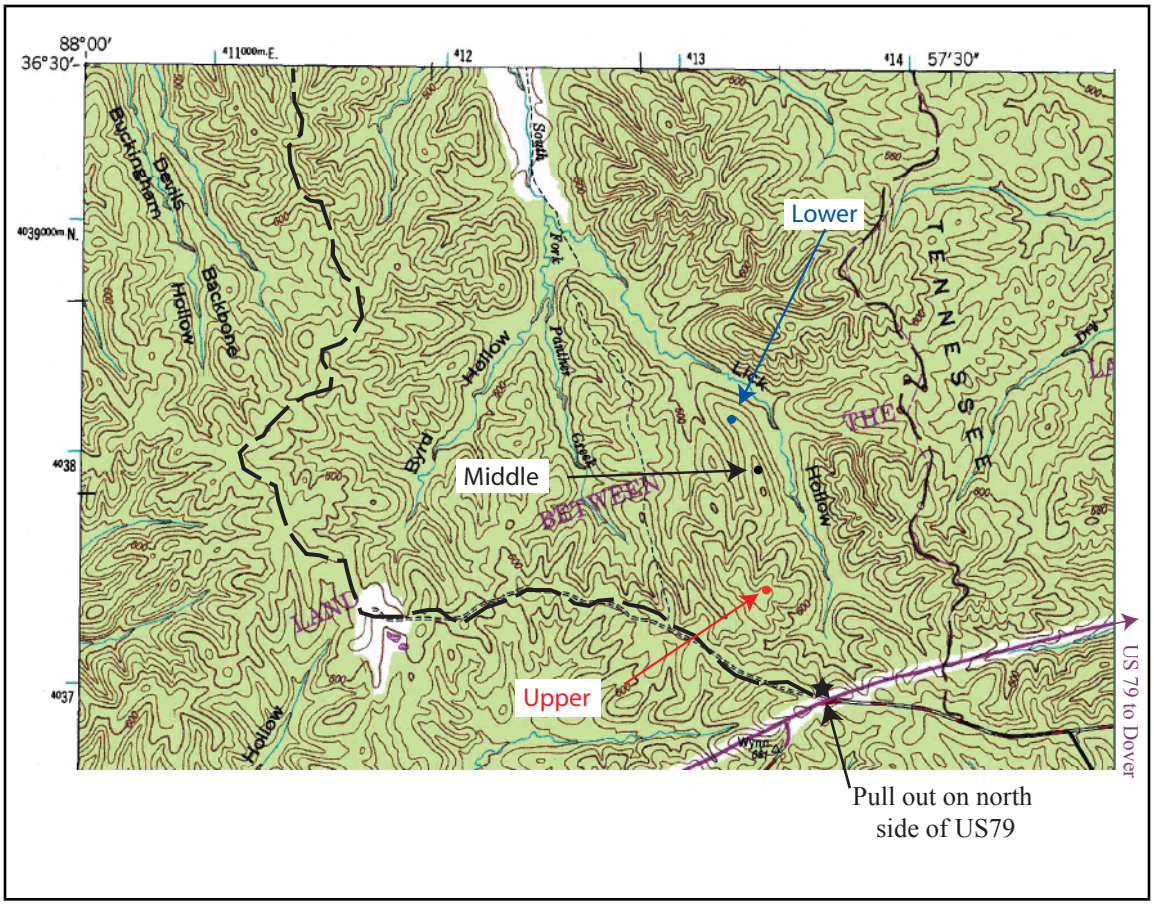

Figure B1-1. Topographic map showin how to get to the hillslopes sampled in this study. This map is the northwest corner of the Standing Rock (TN) USGS topographic map quadrangle.

REFERENCES

Ahnert, F., 1967, The role of the equilibrium concept in the interpretation of landforms of fluvial erosion and deposition, in *L' evolution des Versants*, P. Macar (ed.), 23-41, University of Liege, France.

Anderson, R. S., 2002, Modeling of tor-dotted crests, bedrock edges and parabolic profiles of the high alpine surfaces of the Wind River Range, Wyoming. *Gomorphology*, **46**, 35-58.

Carson, M. A. and Kirkby, M. J., 1972, *Hillslope form and processes*. Cambridge University Press, New York.

Culling, W. E. H., 1963, Soil creep an the development of hillside slopes. *Journal of Geology*, **71**, 127-161.

Feldhamer, G. A.,Whittaker J. C., and Bloemer, S. R., 2002, Often unseen fauna: small mammals and mesocarnivores on Land Between The Lakes, in *Land Between The Lakes, Kentucky and Tennessee: Four Decades of Tennessee Valley Authority Stewardship*, Fralish, J. S., and Chester, E. W. (eds.), 421-435, Austin Peay State University Center for Field Biology, Clarksville, TN.

Fernandes, N. F. and Dietrich, W. E., 1997, Hillslope evolution by diffusive processes: The timescale for equilibrium adjustments. *Water Resources Research,* **33**, 1307-1318.

Franklin, S. B., Robertson, P. A., Fralish, J. S., and Kettler, S. M., 1993, Overstory vegetation and sucessional trends in Land Between The Lakes, USA. *Journal of Vegetation Science*, **4**, 509-520.

Furbish, D. J. and Fagherazzi, S., 2001, Stability of creeping soil and implications for hillslope evolution. *Water Resources Research*, **37**, 2607-2618.

Furbish, D. J., Haff, P. K., Dietrich, W. E., and Heimsath, A. M., 2009, Statistical description of slope-dependent soil transport and the diffusion-like coefficient. *Journal of Geographical Research-Earth Surface*, (in press).

Granger, D. E., Fabel, D., and Palmer, A. N., 2001, Pliocene-Pleistocene incision of the Green River, Kentucky, determined from radioactive decay of cosmogenic ^{26}Al and ^{10}Be in Mammoth Cave sediments.

Harris, S. E., 1988, Summary review of geology of Land Between The Lakes, Kentucky and Tennessee in *Proceedings First Annual Symposium on the Natural History of Lower Tennessee and Cumberland River Valleys*, Snyder, D. H. (ed.), 199-219, Austin Peay State University Center for Field Biology, Clarksville, TN.

Heimsath, A. M., Dietrich, W. E., Nishiizumi, K., and Finkel, R. C., 1997, The soil production function and landscape equilibrium. *Nature*, **388**, 358-361

Heimsath, A. M., Dietrich, W. E., Nishiizumi, K., and Finkel, R. C., 1999, Cosmogenic nuclides, topography, and the spatial variation of soil depth. *Geomorphology*, **27**, 151-172.

Heimsath, A. M., Furbish, D. J., and Dietrich, W. E., 2005, The illusion of diffusion: Field evidence for depth-dependent sediment transport. *Geology*, **33**, 949-952.

Intergovernmental Panel on Climate Change (IPCC), 2007, Climate Change 2007: Synthesis Report.

Lal, R., 2003, Soil erosion and the global carbon budget. *Environment International*, **29**, 437-450.

Lal, R., 2004, Soil carbon sequestration to mitigate climate change. *Geoderma*, **123**, 1-22.

Larson, L.T, and Barnes, R.H., 1965, Mineral resources summary of the Standing Rock quadrangle, Tennessee. State of Tennessee Department of Conservation Division of Geology, Nashville.

Marcher, M.V., 1965, *Geologic map of the Standing Rock quadrangle, Tennessee* [map]. 1:24,000. State of Tennessee Department of Conservation Division of Geology, Nashville.

Marcher, M.V., 1967, *Geologic map of the Tharpe quadrangle, Tennessee* [map]. 1:24,000. State of Tennessee Department of Conservation Division of Geology, Nashville.

Mudd S. M. and Furbish D. J., 2004, Influence of chemical denudation on hillslope morphology. *Journal of Geophysical Research*, **109**(4), doi:10.1029/2003JF000087.

Nash, D, 1980, Forms of bluffs degraded for different lengths of time in Emmet County, Michigan, USA. *Earth Surface Processes*, **5**, 331-345.

NOAA National Weather Service, 2004, Point precipitation frequency estimate (Dover 1 NW, Tennessee), from *Precipitation-Frequency Atlas of the United States: NOAA Atlas 14, Volume 2, Version 3* [Online], Bonnin, G. M., Martin, D., Lin, B., Parzybok, T., Yekta, M., and Riley, D., http://hdsc.nws.noaa.gov/hdsc/pfds/orb/tn_pfds.html accessed March 9, 2009.

Paul, E. A., 2007, *Soil Microbiology, Ecology and Biochemistry*. Academic Press, Boston.

Schimel, D., Stillwell, M.A., and Woodmansee, R. G., 1985, Biogeochemistry of C, N, and P in a soil catena of the shortgrass steppe. *Ecology*, **66**, 276-282.

Stallard, R. F., 1998, Terrestrial sedimentation and the carbon cycle: Coupling weathering and erosion to carbon burial. *Global Biogeochemical Cycles*, **12**, 231-257.

Sundquist, E. T., 1993, The Global Carbon Dioxide Budget. *Science*, **259**, 934-941.

Yoo, K., Amundson, R., Heimsath, A. M., and Dietrich, W. E., 2005, Erosion of upland hillslope soil organic carbon: Coupling field measurements with a sediment transport model. *Global Biogeochemical Cycles*, **19**, doi:10.1029/2004GB002271

Yoo, K., Amundson, R., Heimsath, A.M., and Dietrich, W.E., 2006, Spatial patterns of soil organic carbon on hillslopes: Integrating geomorphic processes and the biological C cycle. *Geoderma*, **130**, 47-65.

BIOGRAPHICAL SKETCH

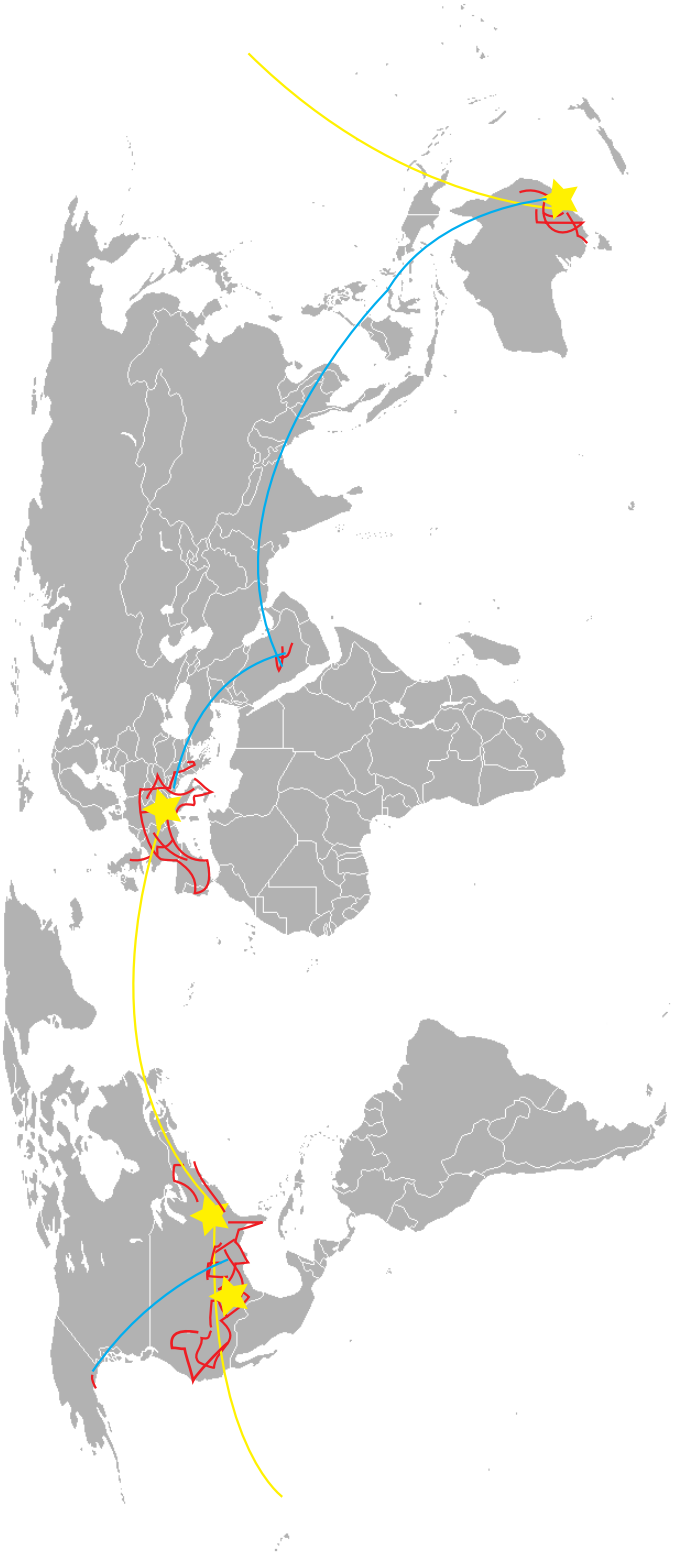

So many more places to go.